DOI: 10.1002/chem.200701331

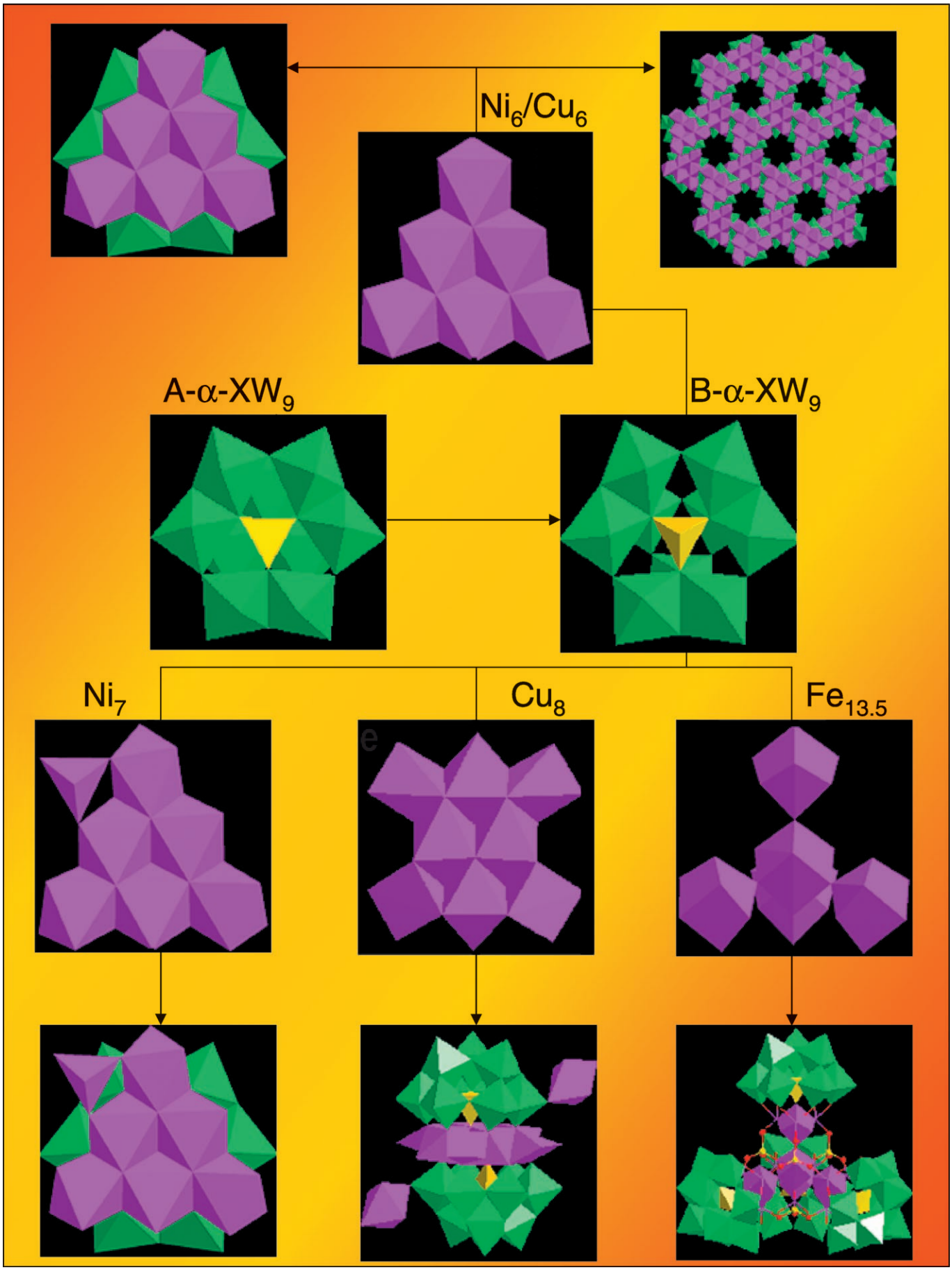

A Combination of Lacunary Polyoxometalates and High-Nuclear Transition-Metal Clusters under Hydrothermal Conditions. Part II: From Double Cluster, Dimer, and Tetramer to Three-Dimensional Frameworks**

Jun-Wei Zhao, Hong-Peng Jia, Jie Zhang, Shou-Tian Zheng, and Guo-Yu Yang*[a]

Abstract: The hydrothermal reactions of trivacant Keggin A-α-XW_9O_{34} polyoxoanions ($X=P^V/Si^{IV}$) with transition-metal ions ($Ni^{II}/Cu^{II}/Fe^{II}$) in the presence of amines result in eight novel high-nuclear transition-metal-substituted polyoxotungstates $[\{Ni_7(\mu_3\text{-}OH)_3O_2(dap)_3(H_2O)_6\}(B\text{-}\alpha\text{-}PW_9O_{34})][\{Ni_6(\mu_3\text{-}OH)_3(dap)_3(H_2O)_6\}(B\text{-}\alpha\text{-}PW_9O_{34})][Ni(dap)_2(H_2O)_2]\cdot 4.5H_2O$ (**1**), $[Cu(dap)(H_2O)_3]_2[\{Cu_8(dap)_4(H_2O)_2\}(B\text{-}\alpha\text{-}SiW_9O_{34})_2]\cdot 6H_2O$ (**2**), $(enH_2)_3H_{15}[\{Fe^{II}_{1.5}Fe^{III}_{12}(\mu_3\text{-}OH)_{12}(\mu_4\text{-}PO_4)_4\}(B\text{-}\alpha\text{-}PW_9O_{34})_4]\cdot ca.130H_2O$ (**3**), $[\{Cu_6(\mu_3\text{-}OH)_3(en)_3(H_2O)_3\}(B\text{-}\alpha\text{-}PW_9O_{34})]\cdot 7H_2O$ (**4**), $[\{Ni_6(\mu_3\text{-}OH)_3(en)_3(H_2O)_6\}(B\text{-}\alpha\text{-}PW_9O_{34})]\cdot 7H_2O$ (**5**), $[\{Ni_6(\mu_3\text{-}OH)_3(en)_2(H_2O)_8\}(B\text{-}\alpha\text{-}PW_9O_{34})]\cdot 7H_2O$ (**6**), $[\{Ni_6(\mu_3\text{-}OH)_3(dap)_2(H_2O)_8\}(B\text{-}\alpha\text{-}PW_9O_{34})]\cdot 7H_2O$ (**7**), and $[\{Ni_6(\mu_3\text{-}OH)_3(en)_3(H_2O)_6\}(B\text{-}\alpha\text{-}SiW_9O_{34})][Ni_{0.5}(en)]\cdot 3.5H_2O$ (**8**) (en = ethylenediamine, dap = 1,2-diaminopropane). These compounds have been structurally characterized by elemental analyses, IR spectra, diffuse reflectance spectra, thermogravimatric analysis, and X-ray crystallography. The double-cluster complex of phosphotungstate **1** simultaneously contains hepta- and hexa-Ni^{II}-substituted trivacant Keggin units $[\{Ni_7(\mu_3\text{-}OH)_3O_2(dap)_3(H_2O)_6\}(B\text{-}\alpha\text{-}PW_9O_{34})]^{2-}$ and $[\{Ni_6(\mu_3\text{-}OH)_3(dap)_3(H_2O)_6\}(B\text{-}\alpha\text{-}PW_9O_{34})]$. The dimeric silicotungstate **2** is built up from two trivacant Keggin $[B\text{-}\alpha\text{-}SiW_9O_{34}]^{10-}$ fragments linked by an octa-Cu^{II} cluster. The main skeleton of **3** is a tetrameric cluster constructed from four tri-Fe^{III}-substituted $[Fe^{III}_3(\mu_3\text{-}OH)_3(B\text{-}\alpha\text{-}PW_9O_{34})]^{3-}$ Keggin units linked by a central $Fe^{II}_4O_4$ cubane core and four μ_4-PO_4 bridges. Complex **4** is an unprecedented three-dimensional extended architecture with hexagonal channels built by hexa-Cu^{II} clusters and trivacant Keggin $[B\text{-}\alpha\text{-}PW_9O_{34}]^{9-}$ fragments. The common feature of **5**–**8** is that they contain a B-α-isomeric trivacant Keggin fragment capped by a hexa-Ni^{II} cluster, very similar to the hexa-Ni^{II}-substituted trivacant Keggin unit in **1**. Magnetic measurements illustrate that **1**, **2**, and **5** have ferromagnetic couplings within the magnetic metal centers, whereas **3** and **4** reveal the antiferromagnetic exchange interactions within the magnetic metal centers. Moreover, the magnetic behavior of **4** and **5** have been theoretically simulated by the MAGPACK magnetic program package.

Keywords: cluster compounds · hydrothermal synthesis · magnetic properties · polyoxometalates · transition metals

Introduction

The search for and discovery of transition-metal-substituted polyoxometalate (TMSP) clusters based on classical lacunary Keggin or Dawson fragments have been extremely intensive interesting owing to the widespread applications in catalysis, material science, medicine, and magnetism.[1] So far, most of the above work focuses on the syntheses of pure inorganic lacunary polyoxometalates (POMs), usually by the conventional aqueous solution method;[2] however, the reaction systems based on lacunary POM precursors and transition-metal complexes (TMC) remain unexplored under hydrothermal conditions. Lately, the hydrothermal technique has been proved to be an extraordinary powerful synthetic method in making new POMs containing saturated

[a] J.-W. Zhao, H.-P. Jia, Prof. Dr. J. Zhang, S.-T. Zheng, Prof. Dr. G.-Y. Yang
State Key Laboratory of Structural Chemistry
Fujian Institute of Research on the Structure of Matter and Graduate School of the Chinese Academy of Sciences
Fuzhou, Fujian 350002 (China)
Fax: (+86) 591-8371-0051
E-mail: ygy@fjirsm.ac.cn

[**] For Part I see: S.-T. Zheng, D.-Q, Yuan, H.-P. Jia, J. Zhang, G.-Y. Yang, *Chem. Commun.* **2007**, 1858

Supporting information for this article is available on the WWW under http://www.chemeurj.org/ or from the author.

polyoxoanions.[3a–d] Although several lacunary polyoxotungstates (POTs) decorated with TMCs[3e–g] were made by hydrothermal treatments of simple tungstates, no systematic investigation of the syntheses of the lacunary POMs as precursors under hydrothermal conditions has been performed. Hence, lacunary POM precursors combined with hydrothermal techniques may provide an easy route to the formation of new TMSPs in the presence of transition-metal (TM) cations. This is because lacunary fragments with high negative charges not only have diverse structural types that can be easily obtained, such as monovacant α-/β-$XW_{11}O_{39}$ and α-$P_2W_{17}O_{61}$, divacant γ-$XW_{10}O_{36}$, trivacant α-/β-XW_9O_{34} (X = Si^{IV}/Ge^{IV}/P^V), α-SbW_9O_{33} and α-$P_2W_{15}O_{56}$ as well as hexavacant α-$H_2P_2W_{12}O_{48}$,[4] but they can also act as good donors to coordinate to electrophiles of TM cations. To develop the synthetic strategy of POMs and synthesize novel TMSPs with good magnetic properties, we extended the synthesis of TMSPs from conventional aqueous solution methods to hydrothermal techniques and are exploring new reaction systems containing lacunary POM fragments, paramagnetic TM cations, and organoamines under hydrothermal conditions. Hydrothermal synthesis[5a–c] is an effective method for growing crystals of numerous inorganic compounds based on the following reasons:

1) The reduced viscosity of water under hydrothermal conditions enhances the diffusion processes so that solvent extraction of solids and crystal growth from solution are favored, thus the formation of good quality crystals is possible.[5a–d] Additionally, the solvent effect under hydrothermal conditions is beneficial for the improved crystallization and the control of the crystal quality, which is helpful for X-ray structural characterization.
2) Hydrothermal conditions are able to make the reaction shift from the thermodynamic to the kinetic so that the equilibrium phases are replaced by structurally more complicated metastable phases,[5e–g] that is, the metastable phases or intermediate phases can easily be captured under hydrothermal conditions.
3) Because solubilities of materials are increased under hydrothermal conditions, a variety of precursors with low solubilities may be introduced to the reaction system. Moreover, a number of organic or inorganic structure-directing or structure-stabilizing agents with appropriate size and shape may be selected for efficient crystal packing during the crystallization process.[5d]
4) Under such nonequilibrium crystallization conditions, the metastable kinetic TMSPs phases rather than the thermodynamic phases are most likely to be captured[5d,e] before lacunary POM precursors are transformed to saturated POM species or are decomposed to other small fragments.

Recently, by using this approach, we have successfully grown single crystals of many novel TMSPs[6] that cannot be made by conventional aqueous solution methods. Our exploratory studies have shown that the hydrothermal environment is suitable not only for making TMSPs, but also for preparing new TMSPs, especially organic–inorganic hybrid TMSPs, that cannot be obtained under conventional aqueous solution methods.

We choose trivacant Keggin A-α-XW_9O_{34} (A-α-XW_9, Figure 1a) fragments as a model reaction based on the following considerations:

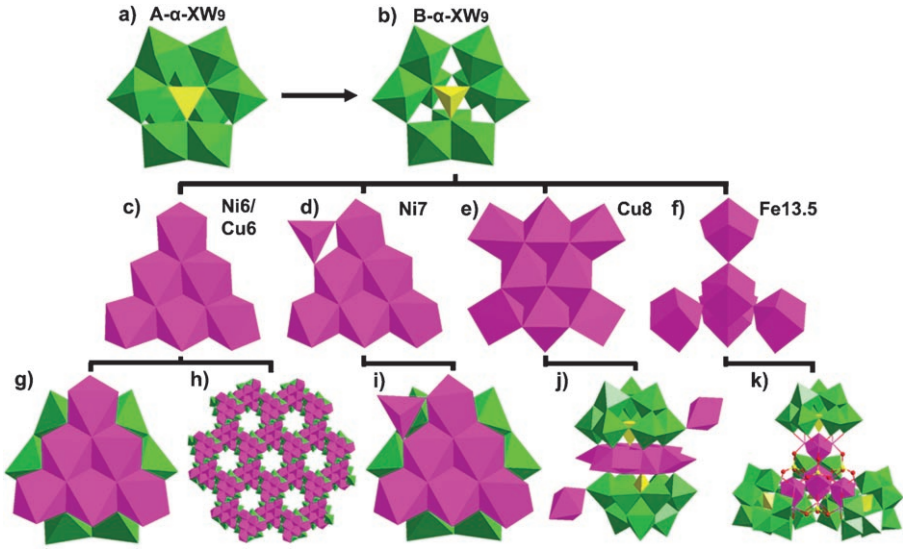

Figure 1. Schematic polyhedral illustration of the isomerization of A-α-XW_9 → B-α-XW_9 and the assembly process of Ni_6/Cu_6, Ni_7, Cu_8 or $Fe_{13.5}$ and B-α-XW_9 SBUs (X = P/Si). The en and dap groups in c)–e) and g)–k) are omitted for clarity.

1) The α-XW_9 unit has relative high stability in diverse lacunary fragments, and its exposed surface oxygen atoms, formed by removal of a W_3O_6 trimer from a saturated Keggin α-$XW_{12}O_{40}$ unit, are available and possess high reaction activity.
2) The lacunary sites of α-XW_9 unit may act as the structure-directing agent (SDA) and induce the formation of TM clusters (Figure 1c–e) or large oligomers of TM clusters (Figure 1f)
3) The subtle combinations between two structural building units (SBUs), trivacant POMs as donors and TM clusters as electrophiles generated in situ, may produce novel high-nuclear TMSPs with isolated, finite polymeric and even extended structures.

4) The hydrothermal reaction can be extended from trivacant Keggin POM fragments to other lacunary POM units.

On the basis of aforementioned points, we have successfully made a series of novel high-nuclear TMSP hybrid clusters **1**–**4** (Figure 1g–k) and some unique trivacant Keggin POTs capped by hexanuclear nickel clusters, **5**–**8**. [{$Ni_7(\mu_3$-$OH)_3O_2(dap)_3(H_2O)_6$}(B-α-PW_9O_{34})][{$Ni_6(\mu_3$-$OH)_3(dap)_3(H_2O)_6$}(B-α-PW_9O_{34})][$Ni(dap)_2(H_2O)_2$]·4.5 H_2O (**1**, [$Ni_7(dap)_3PW_9$][$Ni_6(dap)_3PW_9$]), [$Cu(dap)(H_2O)_3$]$_2$[{$Cu_8(dap)_4(H_2O)_2$}(B-α-$SiW_9O_{34})_2$]·6 H_2O (**2**, [$Cu_8(dap)_4(SiW_9)_2$]), $(enH_2)_3H_{15}$[{$Fe^{II}_{1.5}Fe^{III}_{12}(\mu_3$-$OH)_{12}(\mu_4$-$PO_4)_4$}(B-α-$PW_9O_{34})_4$]· ca.130 H_2O (**3**, [$Fe_{13.5}(PW_9)_4$]), [{$Cu_6(\mu_3$-$OH)_3(en)_3(H_2O)_3$}(B-α-$PW_9O_{34})$]·7 H_2O (**4**, [$Cu_6(en)_3PW_9$]), [{$Ni_6(\mu_3$-$OH)_3(en)_3(H_2O)_6$}(B-α-$PW_9O_{34})$]·7 H_2O (**5**, [$Ni_6(en)_3PW_9$]), [{$Ni_6(\mu_3$-$OH)_3(en)_2(H_2O)_8$}(B-α-$PW_9O_{34})$]·7 H_2O (**6**, [$Ni_6(en)_2PW_9$]), [{$Ni_6(\mu_3$-$OH)_3(dap)_2(H_2O)_8$}(B-α-$PW_9O_{34})$]·7 H_2O (**7**, [$Ni_6(dap)_2PW_9$]), [{$Ni_6(\mu_3$-$OH)_3(en)_3(H_2O)_6$}(B-α-$SiW_9O_{34})$]-[$Ni_{0.5}(en)$]·3.5 H_2O (**8**, [$Ni_6(en)_3SiW_9$]) (en = ethylenediamine, dap = 1,2-diaminopropane). Notice that the A-α-XW_9 (X = P^V/Si^{IV}) (Figure 1a) unit as a starting material was transformed to the B-α-XW_9 (Figure 1b) unit in all the products, indicating that the isomerization of A-α-XW_9→B-α-XW_9 must have taken place during the course of the reactions. Complex **1** not only is a double-cluster complex of POT-containing hexa-/hepta-Ni^{II} clusters incorporated trivacant Keggin units, but it also incorporates the highest number of 3d TM ions in reported trivacant Keggin/Dawson POT monomers to date. Complex **2** is a dimeric TMSP constructed from two trivacant Keggin B-α-SiW_9 units linked by an octa-Cu^{II} cluster. Complex **3** is an unique tetramer containing four tri-Fe^{III} substituted Keggin B-α-PW_9 fragments bridged by a central $Fe^{II}_4O_4$ cubane core and four μ_4-PO_4 bridges. Complex **4** is a three-dimensional framework with an unusual six-connected 4^96^6 topological framework built up of hexa-Cu^{II} clusters and trivacant Keggin B-α-PW_9 fragments. Notably, **4** represents an unprecedented three-dimensional extended architecture with hexagonal channels enclosed by three interweaved helical chains in the POM chemistry. Complexes **5**–**8** are each composed of a B-α-isomeric trivacant Keggin fragment capped by a hexa-Ni^{II} cluster.

Results and Discussion

Synthesis considerations and spectroscopic characterization: Owing to complicated and largely unknown reaction mechanisms, it is quite difficult to design a straightforward synthetic route of the organic–inorganic hybrid TMSP clusters by using conventional aqueous solution methods. Recently, hydrothermal techniques have proved to be an extraordinarily powerful synthetic method for the preparation of one-, two-, and even three-dimensional organic–inorganic hybrid materials in the POM field. In a specific hydrothermal process, many factors can affect the formation and crystal growth of the product phases, such as initial reactants, starting concentration, pH value, reaction time, and temperature, etc. In our case, initial reactants, reactant concentration and temperature greatly influence the crystallization and structural construction of the products.

In the present paper, a series of novel high-nuclear TMSP clusters have been hydrothermally synthesized by the tunable role of the nature of TM ions in the presence of amines (Scheme S1 in the Supporting Information). Initially, an unexpected double-cluster complex simultaneously containing a hepta-/hexa-Ni^{II}-substituted cluster anions [$Ni_6(dap)_3PW_9$]-[$Ni_7(dap)_3PW_9$] (**1**) was obtained by reaction of A-α-PW_9 with $NiCl_2$·6 H_2O at 160 °C in the presence of dap. Here, the excess of $NiCl_2$·6 H_2O was used to enhance its reaction ability with A-α-PW_9 and entailed the reaction shift to the direction of the desired products. Under similar conditions, we expected that using en in place of dap would lead to an isostructural species to **1**; however, we failed to isolate such a product. When the temperature was lowered to 130 and 80 °C, the reaction of A-α-PW_9 with $NiCl_2$·6 H_2O led to two novel hexa-Ni^{II}-encapsulated trivacant Keggin POTs [$Ni_6(en)_2PW_9$] (**6**) and [$Ni_6(en)_3PW_9$] (**5**). Interestingly, the structure of **5** is analogous to the [$Ni_6(dap)_3PW_9$] unit in **1**, while the structure of **6** is very similar to that of **5**, except that two water molecules replace one en ligand in **6**. In the light of the above experimental results, efforts were devoted to obtain the hexa-Ni^{II}-encapsulated compounds with the removal of two or three en ligands and replacing them by four or six water molecules in the asymmetric structural unit by varying the temperature or the amount of en ligand; however, we failed to isolate such complexes. Finally, under the similar synthetic procedure to **6**, replacing en with dap resulted in the formation of [$Ni_6(dap)_2PW_9$] (**7**), which is almost isostructural to **6**. However, to date, the phosphotungstate isostructural to **5** with three dap ligands was not isolated. Subsequently, in order to investigate the influence of the distinct trivacant Keggin polyoxoanion precursors on the structural construction of products, the synthetic procedure used for the preparation of **5** was modified; A-α-SiW_9 was used instead of A-α-PW_9 to afforded [$Ni_6(en)_3SiW_9$] (**8**) and the reported [{$Ni_6(\mu_3$-$OH)_3(dap)_3(H_2O)_6$}(B-α-$SiW_9O_{34})$][$Ni_{0.5}(dap)$]·5 H_2O by our group.[6a] In addition, the isostructural germanotungstates [$Ni(en)_2]_{0.5}$[{$Ni_6(\mu_3$-$OH)_3(en)_3(H_2O)_6$}(B-α-$GeW_9O_{34})$]·3 H_2O and [$Ni_6(dap)_3(H_2O)_6(OH)_3$][B-α-$GeW_9O_{34}$]·$H_3O$·4 H_2O were isolated.[6f] During the course of exploring the reaction of A-α-GeW_9 with $NiCl_2$·6 H_2O, we also obtained a novel two-dimensional tetra-Ni^{II}-sandwiched POT {[$Ni(dap)_2(H_2O)]_2$[$Ni(dap)_2]_2$[$Ni_4(Hdap)_2$(B-α-$HGeW_9O_{34})_2$]}·6 H_2O.[6b] Unfortunately, the double-cluster complexes of silicotungstate or germanotungstate simultaneously containing hepta-/hexa-Ni^{II} units were not obtained, which may be related to the nature of distinct trivacant Keggin polyoxoanion precursors.

To further investigate the assembly mechanism and structural diversity that can be tuned by the nature of different transition-metal ions, we extended our studies from the Ni^{II} ion to the Fe^{II} and Cu^{II} ions. When A-α-PW_9 reacted with

$FeSO_4 \cdot 7H_2O$ at 80 °C, we obtained a brown-prismatic Fe_4O_4-cubane-containing tetramer $[Fe_{13.5}(PW_9)_4]$ (**3**), built up of four tri-Fe^{III}-substituted Keggin units connected by a central $Fe^{II}{}_4O_4$ cubane and four PO_4 groups. However, the tetrameric analogues containing B-α-SiW_9 or B-α-GeW_9 fragments have not been made to date. In the reaction system used for the preparation of complex **5** at 80 °C, when $NiCl_2 \cdot 6H_2O$ is replaced by $CuCl_2 \cdot 2H_2O$, an unprecedented three-dimensional architecture $[Cu_6(en)_3PW_9]$ (**4**) with hexagonal channels was afforded in the hexagonal space group $P6_3$. Also when similar conditions for the reaction system to give **8** were used, but with an elevated of 100 °C and by replacing $NiCl_2 \cdot 6H_2O$ with $CuCl_2 \cdot 2H_2O$, a new dimer $[Cu_8(dap)_4(SiW_9)_2]$ (**2**), constructed from two trivacant Keggin B-α-SiW_9 fragments combined by an octa-Cu^{II} cluster, was formed. Unexpectedly, a novel hexa-Cu^{II}-sandwiched POT $[Cu(enMe)_2]_2\{[Cu(enMe)_2(H_2O)]_2[Cu_6(enMe)_2(B\text{-}\alpha\text{-}SiW_9O_{34})_2]\} \cdot 4H_2O$ was also isolated at 160 °C.[6c] Under the similar conditions used for the preparation of complex **2**, an analogous dimeric germanotungstate $H_4[Cu_8(dap)_4(H_2O)_2(B\text{-}\alpha\text{-}GeW_9O_{34})_2] \cdot 13H_2O$ was also obtained.[6g]

From the systematic exploration of the experimental conditions, the final products of the reaction systems are strongly dependent on the molar ratio of trivacant Keggin precursors/TM ions, the nature of TM ions, and reaction temperature. Thus, the structural differences between **1** and **5**–**6** are mainly controlled by reaction temperature and the amount of A-α-PW_9. The structural variety between **1** and **8** is tuned by the distinct trivacant Keggin precursors. The architecture diversities from **1**, **5**–**7** to **3** and **4** are principally influenced by the nature of TM cations. In addition, under conditions similar to those used in the preparation of **5**, a tetra-Mn^{II}-sandwiched POT $(enH_2)_{10}[Mn_4(H_2O)_2(B\text{-}\alpha\text{-}P\text{-}W_9O_{34})_2]_2 \cdot 20H_2O$ was obtained when the Ni^{II} ion was replaced by the Mn^{II} ion.[6d] Later, when Zn^{II} ions were introduced at 100 °C, two novel two-dimensional tetra-Zn^{II}-sandwiched POTs $[Zn(enMe)_2(H_2O)]_2\{[Zn(enMe)_2]_2[Zn_4(HenMe)_2(PW_9O_{34})_2]\} \cdot 8H_2O$ and $[Zn(enMe)_2(H_2O)]_4[Zn(enMe)_2]_2\{(enMe)_2\{[Zn(enMe)_2]_2[Zn_4(HSiW_9O_{34})_2]\}\{[Zn(enMe)_2(H_2O)]_2[Zn_4(HSiW_9O_{34})_2]\}\} \cdot 13H_2O$ were isolated.[6e] When replacing the Ni^{II} ion with the Co^{II} ion, only pink amorphous powder was obtained. Other TM ions, such as Ti^{IV}, Cr^{III}, and Cd^{II} ions, have also been investigated; however, no analogous species were obtained. In a word, the aforementioned facts indicate that the nickel(II) and copper(II) ions have the high tendency to forming the trivacant Keggin-type POMs anchored by a hexa-/hepta-/octanuclear TM cluster. However, when using triethylenetetramine (teta) or tetraethylenepentamine (tepa) in place of en or dap, only the organic–inorganic hybrid sandwiched structural POTs were obtained, such as $[Ni(tepa)(H_2O)]_4H_2[Ni_4(H_2O)_2(B\text{-}\alpha\text{-}PW_9O_{34})_2] \cdot 8H_2O$.[6e] Nevertheless, the use of 1,3-diaminopropane or 1,6-diaminohexane in place of en or dap led to the formation of amorphous powders. Therefore, organoamines play a key role in the construction of structural diversity under the studied system. In addition, **1**–**8** cannot be obtained by the conventional aqueous solution method by using the same staring materials. In a word, the lacunary sites of α-XW_9 unit may act as the structure-directing agent and induce the formation of TM clusters or large oligomers of TM clusters. In the combination procedure of trivacant α-XW_9 fragments with TM clusters generated in situ, five key factors are concluded as follows:

1) The molar ratio of lacunary POM precursors/TM ions significantly influences the nuclearity number of TM clusters generated in situ and the structural diversity of products; that is, the formations of tetra- or hexa-TM clusters are mainly controlled by the molar ratio of reactants.
2) The nature of different lacunary POM precursors can also tune the nuclearity number of TM clusters generated in situ; that is, the octa-Cu^{II} clusters are only generated by α-SiW_9 or α-GeW_9.
3) The nature of TM ions decides their activity to react lacunary POM precursors; that is, the tetrameric iron-containing POT is only formed by the reaction of Fe^{II} with α-PW_9.
4) The control of temperature can tune the formation of different phases; that is, the preparation of **1**, **5**, and **6** are typical examples.
5) The size and shape of organoamines do not only influence their activity and chelating capability, but also further decide whether they can work as structure-stabilizing agents to enhance the stability of the resulting products.

In fact, these five key factors have been proved in our continuous work. For example, apart from trivacant Keggin POM precursors, monovacant Keggin/Dawson POM and tri-/hexavacant Dawson POM precursors have been introduced to this reaction system and have led to several types of novel and unique TMSPs. The work is in progress and will be reported in due time.

Notably, although the A-α-XW_9 polyoxoanions were used as starting materials, all the products contain the B-α-XW_9 fragments, indicating that the isomerization of A-α-$XW_9 \rightarrow$ B-α-XW_9 must have taken place during the course of the reactions. Such isomerization phenomena have previously been observed under the conventional aqueous solution conditions,[7,4d] and the driving force of isomerization may be the thermodynamic factors.[7c,4d] This isomerization of A-α-$XW_9 \rightarrow$B-α-XW_9 may be closely related to the reaction conditions and the stability of the resulting compounds. On one hand, when the reaction is carried out under heating, isomerization is favored,[7a,c,4d] which is in good agreement with the driving force of isomerization controlled by the thermodynamic factors.[7c,4d] On the other hand, the A-α-XW_9 unit has six exposed surface oxygen atoms at each vacant site, while the B-α-XW_9 unit has seven exposed surface oxygen atoms at each vacant site (Figure 1a,b); hence, the B-α-XW_9 unit can work as a heptadentate ligand to coordinate to the in situ-generated TM clusters and further enhance the stability of the resulting compounds. The follow-

ing experimental facts also proved this viewpoint. For example, in 1986, Knoth et al. demonstrated that A-α-PW_9 can be transformed to B-α-PW_9 in solution in the presence of the first-row TMs upon heating.[7a] When they reacted A-α-PW_9 with divalent first-row TMs in a ratio of about 1:2 at room temperature, they obtained the dimeric polyanions $[M_3(A\text{-}\alpha\text{-}PW_9O_{34})_2]^{12-}$ ($M=Mn^{II}$, Fe^{II}, Co^{II}, Ni^{II}, Cu^{II}, Zn^{II}). However, heating of these solutions above 60 °C resulted in a transformation to the well-known family of tetra-M-sandwiched polyoxoanions $[M_4(H_2O)_2(B\text{-}\alpha\text{-}PW_9O_{34})_2]^{10-}$.[7a] In 1990, Domaille showed that the same isomerization could be accomplished in the solid state.[4d] In 2002, Kortz also observed this isomerization when A-α-PW_9 reacted with the Ni^{II} ion to make $[Ni_3Na(H_2O)_2(B\text{-}\alpha\text{-}PW_9O_{34})_2]^{11-}$.[7c]

In the low-wavenumber regions (Figure S1 in the Supporting Information), IR spectra of **1**–**8** display the characteristic vibration patterns of the trivacant Keggin-type precursors. Four characteristic vibration bands, namely, $\nu(W{-}O_d)$, $\nu(P/Si{-}O_a)$, $\nu(W{-}O_b)$, and $\nu(W{-}O_c)$, appear at 935–967, 1024–1060, 842–875, and 714–798 cm^{-1} for **1** and **3**–**7**, and 939–943, 875–883, 826–836, and 710–778 cm^{-1} for **2** and **8**, respectively. In addition, the appearance of the resonance band centered at 3253–3350 cm^{-1} attributed to the $\nu(N{-}H)$ vibration of amines confirms the presence of organic ammine groups.

To explore the conductivity of compounds **1**–**8**, the measurements of diffuse reflectance spectra for powdered crystal samples were performed to obtain their band gaps (E_g). The band gap was determined as the intersection point between the energy axis and the line extrapolated from the linear portion of the absorption edge in a plot of Kubelka–Munk function against energy E (Figure S2, Table S1 in the Supporting Information).[8a,b] Optical absorption spectra suggest the presence of optical band gaps and semiconductive nature, with large band gaps $E_g=2.88$, 2.74, 2.14, 2.84, 2.95, 2.89, 2.97 and 2.88 eV for **1**–**8**, respectively. These band gaps are related to the energy-level difference between the oxygen π-type HOMO and the tungsten π-type LUMO.[8c] Similar behaviors have been observed in several reported POM-based organic–inorganic hybrid solids, such as $[n\text{-}Bu_4N]_2[Mo_6O_{17}(\equiv NAr)_2$ ($Ar=o\text{-}CH_3OC_6H_4$) ($E_g=$ 2.25 eV),[8c] $[Co_2(bpy)_6(W_6O_{19})_2]$ (bp$y=4$, 4′-bipyridine; ($E_g=2.2$ eV),[8d] $[Cd(bpe)(\alpha\text{-}Mo_8O_{26})][Cd(BPE)(dmf)_4]\cdot$ 2DMF (bpe = 1,2-bis(4-pyridyl)ethane, dmf = *N*,*N*-dimethylformamide) ($E_g=3.45$ eV),[8e] $[Ag_6(3atrz)_6][PMo_{12}O_{40}]_2\cdot H_2O$ ($E_g=1.94$ eV) and $[Ag_2(3atrz)_2]_2[HPMo^{VI}{}_{10}Mo^{V}{}_2O_{40}]$ ($E_g=$ 2.15 eV) (3atr*z* = 3-amino-1,2,4-triazole).[8f] The comparison of their band gaps reveal that they vary only slightly for the those compounds with similar structural types (**1** and **4**–**8**), whereas the change in the band gap is large when the structural type (**2** and **3**) is distinct. In our opinion, these POM-based clusters in the hybrid solids appear to be responsible for their optical band gaps. The variety of the E_g values suggests that the optical band gaps of POM-based clusters can be tuned effectively through the chemical modification by using suitable organic components.

Structural description: Compounds **1**–**8** were only obtained by the hydrothermal reaction of trivacant Keggin A-α-XW_9 precursors and TM salts in the presence of en or dap, and not made by the conventional aqueous solution method at atmosphere pressure. Systematic investigation on the synthetic conditions proved that in the absence of en or dap only well-known sandwich-type POMs[2e,9] or amorphous powders were obtained, indicating that en or dap played a key role in the formation of **1**–**8**. All above compounds can be reproducibly synthesized in a good yield under hydrothermal conditions.

$[Ni_7(dap)_3PW_9][Ni_6(dap)_3PW_9]$ (1): Compound **1** is a unique double-cluster complex (Figure 2a) of phosphotungstate containing both hexa- and hepta-Ni^{II}-substituted trivacant Keggin clusters of $\{Ni_6(dap)_3PW_9\}$ (Figure 1g) and $\{Ni_7(dap)_3PW_9\}$ (Figure 1i). Both $\{Ni_6(dap)_3PW_9\}$ and $\{Ni_7(dap)_3PW_9\}$ clusters consist of two SBUs, the well-known trivacant B-α-PW_9 fragment[10] and a new $\{Ni_6(dap)_3\}$/$\{Ni_7(dap)_3\}$ unit. The $\{Ni_6(dap)_3\}$ unit (Figure 3) contains a hexa-Ni^{II} $[Ni_6(\mu_3\text{-}OH)_3]^{9+}$ core surrounded by the trivacant sites of the B-α-PW_9 unit; the core is made up of six nearly coplanar Ni^{II} ions in a triangle motif linked together by three μ_3-OH bridges ($Ni{-}\mu_3\text{-}O_{OH}$: 1.990(3)–2.049(2) Å), and stabilized by six μ_3-O bridges from six WO_6 octahedra ($Ni{-}\mu_3$-O: 2.039(2)–2.159(3) Å) and one μ_4-O bridge from the central PO_4 tetrahedron ($Ni{-}\mu_4$-O: 2.145(2)–2.171(2) Å), subsequently the octahedral coordination sphere of each Ni^{II} ion is completed by dap or water ligands (Ni–N: 2.047(4)–2.091(3) Å and $Ni{-}O_W$: 2.049(2)–2.129(3) Å). In the hexa-Ni^{II} $[Ni_6(\mu_3\text{-}OH)_3]^{9+}$ core, each of three interior Ni atoms (Ni11–Ni13) is located at the trivacant sites of the B-α-PW_9 unit and bond to one water molecule, while each of three exterior Ni atoms (Ni8–Ni10) coordinates to one bidentate dap and one water ligand, respectively, resulting in the formation of the $\{Ni_6(dap)_3\}$ cluster unit (Figure 1c and3b). This $\{Ni_6(dap)_3\}$ unit caps to the B-α-PW_9 unit through exposed seven O atoms from six WO_6 octahedra and one PO_4 tetrahedron, forming a novel hexanuclear Ni_6-incorporated large neutral cluster $\{Ni_6(dap)_3PW_9\}$ (Figure 1g). Three μ_3-OH bridges and six terminal water molecules are localized by bond valence sum (BVS) calculations.[11a] In addition, the distribution motif of the six octahedral Ni^{II} ions exhibits a completely triangular arrangement: three exterior Ni (Ni_{ex}) atoms are situated in three corners of the triangle with $Ni_{ex}\cdots Ni_{ex}$ distances of 6.224(8)–6.238(8) Å, another three interior Ni (Ni_{in}) atoms are positioned on the midpoints of three edges with $Ni_{in}\cdots Ni_{in}/Ni_{ex}\cdots Ni_{in}$ separations of 3.103(5)–3.132(7) Å. Alternatively, the distribution motif of the $[Ni_6(\mu_3\text{-}OH)_3]^{9+}$ core is also considered as three edge-sharing truncated cubanes, $Ni_3O_3(OH)$ (Figure 2b). The hepta-Ni^{II}-substituted $\{Ni_7(dap)_3PW_9\}$ cluster (Figure 3a) can be viewed to be formed by two O atoms of the $Ni7O_2(H_2O)_2$ tetrahedron replacing the terminal water ligands on Ni8 and Ni12 ions in $\{Ni_6(dap)_3PW_9\}$ cluster accompanying the reversal of the coordination orientation of the dap ligands on Ni8 and Ni10 ions (Figure 3a,b). Interestingly, the two negative

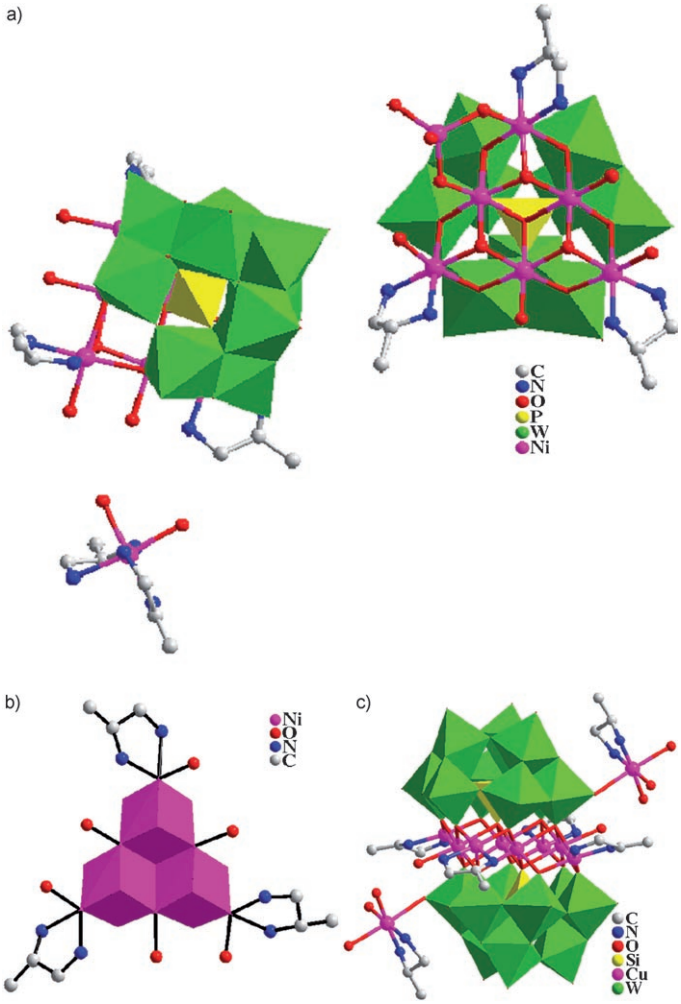

Figure 2. a) Polyhedral/ball-and-stick representation of **1**. b) The distribution motif of the $[Ni_6(\mu_3\text{-}OH)_3]^{9+}$ core as three edge-sharing truncated cubanes, $Ni_3O_3(OH)$. c) Side view of molecular unit built from two B-α-SiW_9 fragments and the Cu_8 cluster core in **2**. All hydrogen atoms and crystal water molecules were omitted for clarity. For **1**, W–O_t: 1.675(12)–1.735(12) Å, W–$O_{b(c)}$: 1.839(13)–2.015(11) Å, W–O_a: 2.400(10)–2.504(11) Å, W–O_{Ni}: 1.787(11)–1.823(11) Å, P–O: 1.529(10)–1.567(11) Å, Ni–O: 1.903(15)–2.261(11) Å for octahedral geometry, Ni–O: 1.870(9)–1.939(10) Å for tetrahedral geometry, Ni–N: 2.009(17)–2.19(3) Å. For **2**, W–O_t: 1.699(8)–1.727(8) Å; W–$O_{b(c)}$: 1.877(7)–1.975(7) Å; W-O_a: 2.309(7)–2.430(6) Å; W–O_{Cu}: 1.716(7)–1.877(7) Å; Si–O: 1.638(7)–1.643(7) Å; Cu–O: 1.956(6)–2.38(5) Å and Cu–N: 1.88(3)–1.89(2) for octahedral geometry; Cu–O: 1.971(7)–2.404(7) Å and Cu–N: 1.962(9)–2.001(10) Å for square pyramidal geometry.

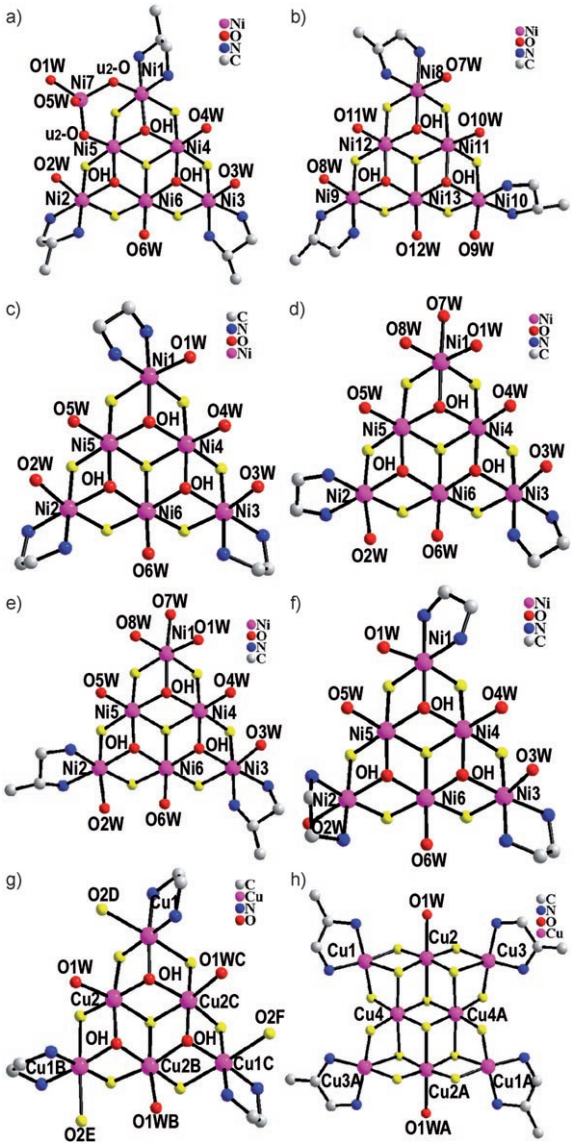

Figure 3. Ball-and-stick illustrations of a) Ni_7, b) Ni_6 cores in **1**, c) Ni_6 core in **5**, d) Ni_6 core in **6**, e) Ni_6 core in **7**, f) Ni_6 core in **8**, g) Cu_6 core in **4** and h) Cu_8 core in **2** with selected numbering scheme and yellow oxygen atoms from B-α-XW_9 fragments. The atoms with "A", "B", "C", "D", "E", or "F" in their labels were symmetrically generated (A: $1-x$, $2-y$, $1-z$; B: $3-y$, $2+x-y$, z; C: $1-x+y$, $3-x$, z; D: $3-x$, $3-y$, $0.5+z$; E: y, $2-x+y$, $0.5+z$; F: $1+x-y$, x, $0.5+z$). All hydrogen atoms were omitted for clarity.

charges of the $\{Ni_7(dap)_3PW_9\}$ cluster are balanced by a $[Ni(dap)_2(H_2O)_2]^{2+}$ ion. Moreover, these water and diamine ligands provide good electron donors for the derivation of the supramolecular interactions through hydrogen bonds (Table S2 in the Supporting Information). Although the tri-/tetra-Ni^{II}-substituted trivacant Keggin POTs, $[Ni_3(H_2O)_3PW_{10}O_{39}(H_2O)]^{7-}$[2e] and $[H_2PW_9Ni_4O_{34}(OH)_3(H_2O)_6]^{2-}$[12] have been reported, the hepta-Ni^{II}-substituted trivacant Keggin POT **1** is, to the best of our knowledge, reported here for the first time.

$[Cu_8(dap)_4(SiW_9)_2]$ (2): In contrast to compound **1**, compound **2** consists of two B-α-SiW_9 fragments and a $\{Cu_8(dap)_4\}$ unit (Figures 1j, and 2c), with two pendant $[Cu(dap)(H_2O)_3]^{2+}$ cations; to the best of our knowledge this not only represents a novel octa-TM cluster $\{Cu_8\}$, but also has the greatest number of 3d TM cations sandwiched in the trivacant Keggin or Dawson POM dimers of those reported to date. In the structure of **2**, two trivacant Keggin B-α-SiW_9 fragments are staggered with respect to each other and are linked by a $\{Cu_8(dap)_4\}$ cluster (Figure 2c) through eight μ_3-O and four μ_4-O atoms from the lacunae of the B-α-SiW_9

fragments as well as two central μ_4-O atoms from two SiO_4 tetrahedra. The distribution motif of the eight Cu^{II} ions in the form of 3:2:3 leads to three types of the coordination environments of Cu^{II} ions (Figure 3h): the first type (Cu1, Cu1A, Cu3, Cu3A) resides in a five-coordinate square pyramid, in which the basal plane is defined by two nitrogen atoms from a bidentate dap ligand (Cu–N: 1.962(9)–2.001(10) Å) and two μ_3-O atoms from the lacunae of two B-α-SiW_9 fragments (Cu–μ_3-O: 1.971(7)–2.003(7) Å), and one μ_4-O atom from the lacunae of a B-α-SiW_9 fragment occupies the apical position (Cu–O: 2.358(7)–2.404(7) Å); the second type (Cu2, Cu2A) is a six-coordinate octahedral geometry with two μ_3-O and two μ_4-O atoms from the lacunae of two B-α-SiW_9 fragments building the equatorial plane (Cu–μ_3-O: 1.956(6)–1.978 (7) Å and Cu–μ_4-O: 1.978(7)–1.988(7) Å], and one μ_4-O atom from a SiO_4 tetrahedron and one water O atom standing on the axial positions (Cu–μ_4-O: 2.376(7) Å and Cu–O_W: 2.317(9) Å]; the third type (Cu4 and Cu4 A) also adopts an octahedral geometry with two μ_3-O and two μ_4-O atoms from the lacunae of two B-α-SiW_9 fragments building the equatorial plane (Cu–μ_3-O: 1.951(7)–1.981 (7) Å and Cu–μ_4-O: 1.982(6) Å), and two μ_4-O atoms from the lacunae of two B-α-SiW_9 fragments in the axial positions (Cu–μ_4-O: 2.361(7)–2.3614(7) Å). Additionally, adjacent Cu···Cu separations range from 2.980(1)–3.186(1) Å. Note that the occurrence of **2** not only enriches the dimeric POM chemistry, but also provides a novel synthetic method for incorporating much more 3d TM cations between two trivacant Keggin or Dawson POM fragments.

$[Fe_{13.5}(PW_9)_4]$ (3): The large $\{Fe_{13.5}(PW_9)_4\}$ cluster in **3** about 18.2×20.0 Å in size (Figures 1k and 4a,b), is a new member of poly(POM) family.[2e,13–19] Its main skeleton is a tetrameric poly(POM) with an approaching T_d symmetry, which contain four tri-Fe^{III} substituted $[Fe^{III}_3(\mu_3\text{-}OH)_3(B\text{-}\alpha\text{-}PW_9O_{34})]^{3-}$ ($\{Fe_3PW_9\}$) Keggin units linked by a central $Fe^{II}_4O_4$ cubane core and four μ_4-PO_4 bridges (Figure 4c). Each μ_4-PO_4 unit links four vertex-sharing $Fe_4(O,OH)_4$ cubanes (one central $Fe^{II}_4O_4$ and three $Fe^{III}_3Fe^{II}O(OH)_3$, Figure 4d). Note that four O vertices of the $Fe^{II}_4O_4$ core come from four μ_4-PO_4 bridges. Each $\{Fe_3PW_9\}$ unit links not only to one Fe^{II} vertex of the central $Fe^{II}_4O_4$ core through three μ_3-OH bridges from the $\{Fe_3PW_9\}$ unit, but also to three O vertices of the $Fe^{II}_4O_4$ core through three P atoms, respectively (Figure 4e).

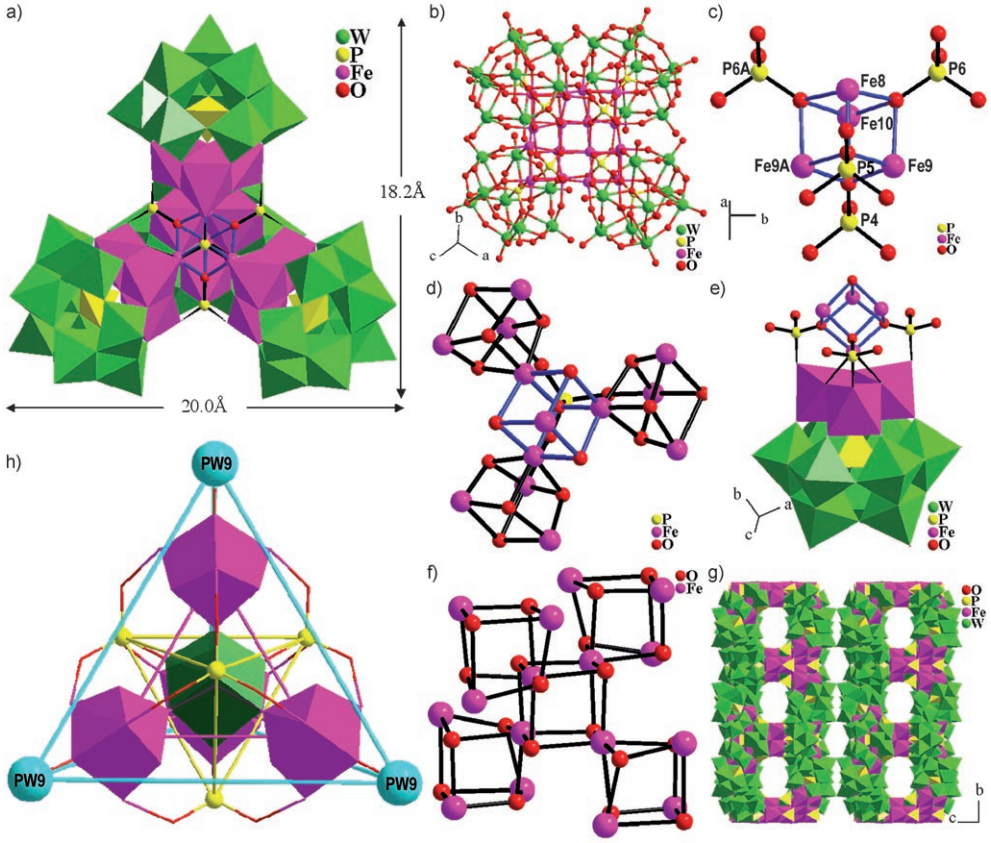

Figure 4. a) and b) Polyhedral/ball-and-stick representations of the tetrameric Keggin poly(POM) **3**. The water and protonated en molecules were omitted for clarity. c) Combination of the central $Fe^{II}_4O_4$ core and four PO_4 bridging groups. The atoms with "A" in their labels were symmetrically generated (A: x, $-y$, z).d) Coordination environment of one PO_4 group linking one central $Fe^{II}_4O_4$ and three $Fe^{III}_3Fe^{II}O(OH)_3$ cubanes. e) The connection motif of the $\{Fe_3PW_9\}$ unit, the central $Fe^{II}_4O_4$ core and three PO_4 groups. f) Four $\{Fe_3\}$ trimers of $\{Fe_3PW_9\}$ units linking the central $Fe_4{}^{II}O_4$ cubane to form a $\{Fe_{13.5}\}$ cluster containing one interior $Fe_4{}^{II}O_4$ and four exterior $Fe^{III}_3Fe^{II}O(OH)_3$ cores. g) The polyhedral stacking of **3** along the *a* axis shows two types of elliptical channels with the sizes of 10.8×19.8 Å and 6.3×9.5 Å, respectively. h) Polyhedral/ball-and-stick view of the linking model of $Fe^{III}_3Fe^{II}O(OH)_3$ cubanes (purple), $Fe^{II}_4O_4$ cubane (green), PW_9 (cyan) and PO_4 groups (yellow) in **3**.

Thus, four $\{Fe_3\}$ trimers of $\{Fe_3PW_9\}$ units combine with the central $Fe^{II}{}_4O_4$ cubane to form a $\{Fe_{13.5}\}$ cluster containing five $Fe_4(O,OH)_4$ cubanes sharing Fe^{II} vertices with each other (one interior $Fe^{II}{}_4O_4$ and four exterior $Fe^{III}{}_3Fe^{II}O(OH)_3$ cores, Figure 4f). If each B-α-PW_9 unit acts as a node, four B-α-PW_9 units are situated in the four vertices of a tetrahedron (Figure 4h). The interior $Fe^{II}{}_4O_4$ cubane resides in the center of this tetrahedron, while four exterior $Fe^{III}{}_3Fe^{II}O(OH)_3$ cubanes are located just inside the four pyramidal angles. Intriguingly, four μ_4-PO_4 groups are located exactly at the center of four faces of the tetrahedron. It differs markedly from the tetrameric $[Nb_4O_6(\alpha\text{-}Nb_3SiW_9O_{40})_4]^{20-}$ tetramer[14] in which each $[\alpha\text{-}Nb_3SiW_9O_{40}]^{7-}$ Keggin unit joins to three Nb atoms located on one face of the $[Nb_4O_6]^{8+}$ tetrahedral core through three Nb-O-Nb bonds. Thus, the connection modes between the $Fe^{II}{}_4O_4$ core and four tri-Fe^{III}-substituted $\{Fe_3PW_9\}$ units in **3** are unique in the poly(POM) family.[2e,13–19] The M_4O_6 core has been reported in several complexes,[14,20] while the M_4O_4 cubane has only been observed in a $[(Cp^*Nb)_4O_4]$ complex containing Nb^{IV} centers reduced from the Nb^{V} centers.[20c] Unlike the Nb^{IV} centers in $[(Cp^*Nb)_4O_4]$[20c] and the Nb^{V} centers in $[Nb_4O_6(\alpha\text{-}Nb_3SiW_9O_{40})_4]^{20-}$,[14] the $\{Fe_{13.5}(PW_9)_4\}$ cluster contains mixed Fe^{II} and Fe^{III} centers: Fe^{II} centers in the Fe_4O_4 core and Fe^{III} centers, formed from the oxidation of Fe^{II} centers, in the trivacant sites of $[Fe_3(\mu_3\text{-}OH)_3(B\text{-}\alpha\text{-}PW_9O_{34})]^{3-}$ units. Alternatively, the $\{Fe_{13.5}(PW_9)_4\}$ tetramer may also viewed as four $[B\text{-}\alpha\text{-}PW_9O_{34}]^{9-}$ units anchored by a $[Fe^{II}{}_{1.5}Fe^{III}{}_{12}(\mu_3\text{-}OH)_{12}(\mu_4\text{-}PO_4)_4]^{15+}$ core, such a large Fe-P-O polymeric cation containing five vertex-sharing cubanes and four PO_4 groups is first observed in a isolated molecule. Owing to the approaching T_d symmetry for the tetramer, there are three sets of tetrahedral topologies in the $\{Fe_{13.5}(PW_9)_4\}$ cluster, corresponding to four B-α-PW_9 fragments, four $Fe^{III}{}_3Fe^{II}O(OH)_3$ cubanes, and four PO_4 groups (Figure 4h). The $Fe^{II}{}_4O_4$ cubane resides in the center of three tetrahedra. In addition, the $\{Fe_{13.5}(PW_9)_4\}$ cluster are stacked along the *a* axis, forming two types of channels with the dimensions of 10.8×19.8 and 6.3×9.5 Å, in which the solvent water molecules are filled (Figure 4g).

In the $[Fe^{II}{}_{1.5}Fe^{III}{}_{12}(\mu_3\text{-}OH)_{12}(\mu_4\text{-}PO_4)_4]^{15+}$ unit, the BVS calculations show that the oxidation states of all octahedral Fe centers can be classified into two types: the Fe1–Fe7 atoms on the lacunae of four B-α-PW_9 units and the Fe8–Fe10 atoms in the central Fe_4O_4 cubane are +3 (Fe^{III}–O: 1.86(2)–2.38(2) Å) and +2 (Fe^{II}–O: 2.02(2)–2.22(2) Å), respectively;[11b] this assignment was also confirmed by X-ray photoelectron spectroscopy (Figure S3 in the Supporting Information). In **3**, the $Fe2p_{1/2}$ and $Fe2p_{3/2}$ binding energy values of 725.9 and 713.9 eV indicate the presence of the Fe^{III} centers, while the $Fe2p_{1/2}$ and $Fe2p_{3/2}$ binding energy values of 723.1 and 709.8 eV reveal the presence of the Fe^{II} centers. These values are in good agreement with the values found in the literature.[21] The P4–P6 atoms are disordered and split into two positions, while the Fe8–Fe10 atoms only occupy 0.25 of the sites based on the rationality of their atomic thermal displacement parameters, which is in agreement with the results of inductively coupled plasma (ICP) and energy-dispersive X-ray analysis (EDXA). Furthermore, compound **3** is highly hydrated, so that when it is exposed to the X-ray beam for the collection of intensity data, the water molecules of crystallization are easily lost from the structure. Therefore, some water molecules of crystallization cannot be directly determined by X-ray diffraction. A combination of elemental analysis and thermogravimetric analysis (Figure S4) confirms the number of water molecules of crystallization in **3**, which is not uncommon in giant poly(POM) species.[13]

So far, although several poly(POM) species have been reported, such as trimer $[Ni_9(OH)_3(H_2O)_6(HPO_4)_2(PW_9O_{34})_3]^{16-}$,[2e] tetramers $[\{(SiW_9O_{34})(SiW_9O_{33}(OH))(Cu(OH))_6Cu\}_2X]^{23-}$ (X = Cl, Br),[13] $[Nb_4O_6(\alpha\text{-}Nb_3SiW_9O_{40})_4]^{20-}$,[14] $[PM_2W_{10}O_{38}]_4(W_3O_{14})]^{30-}$ (M = Eu, Y),[15] $[\{Ti_3P_2W_{15}O_{57.5}(OH)_3\}_4]^{24-}$,[16] $[\{\beta\text{-}Ti_2SiW_{10}O_{39}\}_4]^{24-}$,[17a] $[Cu_{20}Cl(OH)_{24}(H_2O)_{12}(P_8W_{48}O_{184})]^{25-}$,[17c] $[H_{56}P_8W_{48}Fe_{28}O_{248}]^{28-}$,[18a] $[H_{55}P_8W_{49}Fe_{27}O_{248}]^{26-}$,[18a] and $[KFe_{12}(OH)_{18}(\alpha\text{-}1,2,3\text{-}P_2W_{15}O_{56})_4]^{29-}$[18b] as well as two dodecamers $[\{Sn(CH_3)_2\}_2(H_2O)_{24}\{Sn(CH_3)_2\}_{12}(A\text{-}XW_9O_{34})_{12}]^{36-}$ (X = P, As),[17b] and $[As_{12}Ce_{16}(H_2O)_{36}W_{148}O_{524}]^{76-}$,[19] these poly(POM) species were mostly obtained by the conventional aqueous solution method. Here **3** is an unique poly(POM) species in POM chemistry, as it is formed under hydrothermal conditions. To date, some novel poly(POM) species, from isolated, finitely polymeric and one-dimensional chains[6a] to three-dimensional frameworks (see below, compound **4**), have been made in our laboratory under hydrothermal conditions.

$[Cu_6(en)_3PW_9]$ (4): Compound **4** is a novel three-dimensional framework constructed from trivacant Keggin POM fragments and hexa-Cu^{II} clusters (Figures 1h and 5, and Figure S8 in the Supporting Information). Such an example has not been made by conventional aqueous solution methods. The large neutral cluster unit $\{Cu_6(en)_3PW_9\}$ in **4** is different from the $\{Ni_6(en)_3PW_9\}$ unit in **5** (Figure 3c–f and Figures S5–S7 in the Supporting Information for **5**–**8**), although the backbones of the hexanuclear $\{M_6(en)_3\}$ clusters are similar in **4** and **5**. In **5**, each of three exterior Ni atoms in the $\{Ni_6(en)_3\}$ unit binds to one water ligand (Figure 3c and Figure S5 in the Supporting Information), while three terminal water ligands of three exterior Cu atoms in $\{Cu_6(en)_3\}$ unit of **4** are substituted by three terminal O atoms from three adjacent B-α-PW_9 units (Figure 3g and Figure S8 in the Supporting Information). Furthermore, each B-α-PW_9 unit also joins three $\{Cu_6(en)_3\}$ clusters (Figure 5a). Thus, each large $\{Cu_6(en)_3PW_9\}$ SBU as a complete cluster unit connects six such SBUs through six Cu-O-W linkages (Figure 5b) to form an unprecedented three-dimensional framework with hexagonal channels of dimensions of 5.6×5.6 Å (Figure 5c). Interestingly, each hexagonal channel is enclosed by three interweaved helices (Figure 5d–f). The helical chains along the 6_3 screw axis are constructed from the $\{Cu_6(en)_3PW_9\}$ SBUs through the Cu-O-W linkages. All the hexagonal helical channels are connected through the square-like windows surrounded by four $\{Cu_6(en)_3PW_9\}$ SBUs (Figure 5e,f). Such

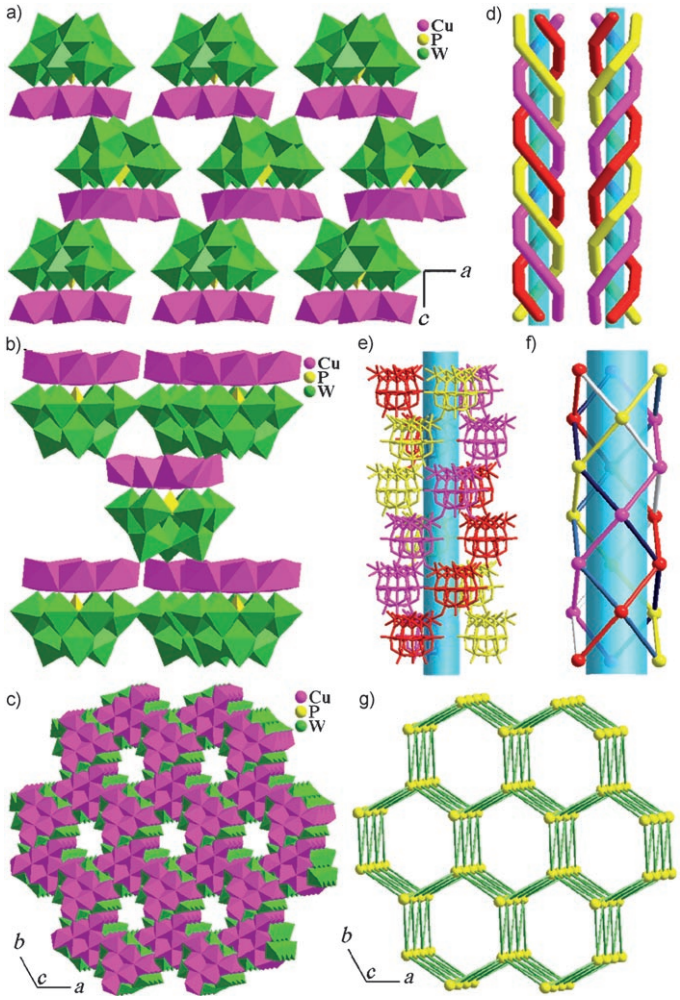

Figure 5. a) The staggered arrangement of the $[Cu_6(en)_3PW_9]$ units in the -ABAB- mode along the *c* axis. The lattice water molecules, and the carbon and hydrogen atoms were omitted for clarity, similarly hereinafter. b) The coordination environment of each $[Cu_6(en)_3\ PW_9]$ SBU connecting six the same SBUs through six Cu-O-W linkages. c) The hexagonal channels in **4** viewed along the *c* axis. d) The left-/right-handed helices enclosing a hexagonal channel. Triple helical chains are marked with red, purple and yellow. e) The tubular channel constructed from triple-helical chains (red, yellow, and purple) made from the $[Cu_6(en)_3PW_9]$ SBUs through the Cu-O-W bridges along the 6_3 screw axis, generating the hexagonal channel and square-like windows in **4**. f) The topological view of the tubular channel made of interweaving two sets of triple-helical chains: one contains yellow, purple, and red lines, the other consists of white, blue, and cyan lines, respectively. g) Archimedean-type six-connected three-dimensional topological net along the *c* axis. The yellow balls are six-connected nodes on behalf of $[Cu_6(en)_3PW_9]$ units.

helical channels built by interweaved helical chains are very rare in POM chemistry.[22] In the structure of **4**, the $\{Cu_6(en)_3PW_9\}$ SBUs are staggered in the -ABAB- mode along the *c* axis (Figure 5a). From the topological point of view, the three-dimensional framework of **4** is a six-connected network, belonging to the "Archimedean-type" three-dimensional net,[23] in which each $\{Cu_6(en)_3PW_9\}$ SBU acts as a six-connected node (Figure 5g). A topological analysis of this net was performed with OLEX.[24] The long topological (O'Keeffe) vertex symbol is $4{\cdot}4{\cdot}4_2{\cdot}4{\cdot}4_2{\cdot}4{\cdot}4{\cdot}4{\cdot}4_2{\cdot}6_4{\cdot}6_4{\cdot}6_4{\cdot}6_4{\cdot}6_4{\cdot}6_4$ for the $\{Cu_6(en)_3PW_9\}$ node, which gives the short vertex (Schäfli) symbol 4^96^6. The novel poly(POM) species with the extended structures obtained under hydrothermal conditions indicates that the flexible coordination modes of M_6 clusters and B-α-PW_9 fragments play a key role in the formation of one-dimensional chain made by $\{Ni_6(dien)_3PW_9\}$ SBUs[6a] (dien = diethylenetriamine) and three-dimensional framework built by $\{Cu_6(en)_3PW_9\}$ SBUs. In the one-dimensional chain structure, each $\{Ni_6(dien)_3PW_9\}$ SBU acts as a two-connected node;[6a] while in the three-dimensional framework of **4**, each $\{Cu_6(en)_3PW_9\}$ SBU functions as a six-connected node.

Structures of 5–8: Compounds **5–8** consist of B-α-XW_9 fragments and Ni_6-containing units (Figures 1g and 3c–f, and Figures S5–S7 in the Supporting Information). Because the Ni_6-containing units in **5–8** are very analogous to the Ni_6-containing unit in **1**, we will not discuss them again in great detail. However, it is worth noting that the coordination environment of $\{Ni_6(en)_3\}$ cluster in **5** (Figure 3c) is somewhat different from that of the $\{Ni_6(dap)_3\}$, $\{Ni_6(en)_2\}$, and $\{Ni_6(dap)_2\}$ clusters in **1**, **6**, and **7**, respectively. For compound **5**, three en ligands coordinate to three exterior Ni atoms (Figure 3c). In contrast to **5**, three dap ligands coordinate to three exterior Ni atoms in **1** (Figure 3b); two water molecules in **6** replace one en ligand of the Ni1 atom (Figure 3d), whereas in **7**, two water molecules coordinate to Ni1 atom and two dap ligands coordinate to Ni2 and Ni3 atoms (Figure 3e). In the case of **8**, the $\{Ni_6(en)_3\}$ cluster is almost isostructural to that of **5** except the coordination orientation of en ligands (Figure 3f); unlike **5–7**, the trivacant Keggin fragment in **8** is B-α-SiW_9, thus the $[Ni_{0.5}(en)]^+$ cation is need for the charge balance in **8** (Figure S7 in the Supporting Information). By a close inspection, the coordination water molecules and amine ligands in Ni_6-containing units have different orientations in **1** and **5–8**.

Magnetic properties: The magnetic susceptibilities of **1–5** were measured at 2–300 K. The plot of $\chi_M T$ versus T of **1** under a constant magnetic field of 10 kOe is shown in Figure 6. The value of $\chi_M T$ at 300 K is 16.93 emu mol^{-1} K, consistent with the spin-only value expected for fourteen non-correlated $S=1$ Ni^{II} ions with $g=2.2$. Upon cooling, $\chi_M T$ increases to a maximum of 37.59 emu mol^{-1} K at 13 K. This magnetic behavior typifies the ferromagnetic coupling interactions between adjacent Ni^{II} centers, which is confirmed by the positive Weiss constant $\theta = 14.17$ K (Figure S9 in the Supporting Information). A sudden decrease of $\chi_M T$ value below 13 K suggests the presence of the significant zero-field- splitting (ZFS) effects in the ground state and/or antiferromagnetic intercluster interactions.[25] Within the two $\{Ni_6(dap)_3\}$ and $\{Ni_7(dap)_3\}$ clusters in **1**, the exchange couplings between adjacent Ni^{II} ions are mainly transmitted through the μ_2-O, μ_3-O, and μ_3-OH and μ_4-O bridges. Except the Ni7-O-Ni1 and Ni7-O-Ni5 angles, the Ni-O-Ni bond angles are in the range of 91.7–105.2° at which the Ni···Ni ferromagnetic exchange interactions are dominant (90±

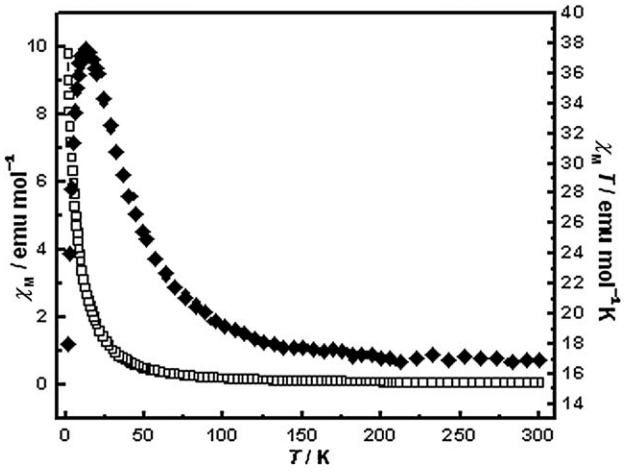

Figure 6. The temperature dependence of the molar magnetic susceptibility χ_M (■) and the product of the molar magnetic susceptibility and temperature $\chi_M T$ (◆) for **1** between 2 and 300 K.

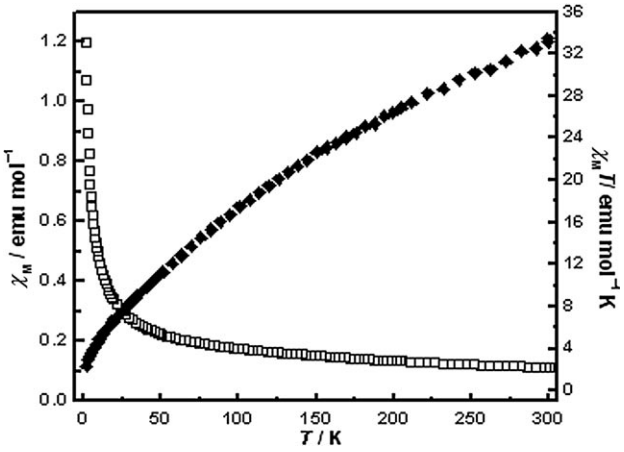

Figure 7. The temperature dependence of the molar magnetic susceptibility χ_M (□) and the product of the molar magnetic susceptibility and temperature $\chi_M T$ (◆) for **3** between 2 and 300 K.

14°).[26] Thus dominant ferromagnetic exchange interactions are not unexpected in this system.

The magnetic behavior of **2** is similar to that of **1** (Figure S10 in the Supporting Information). The $\chi_M T$ product of 5.10 emu mol^{-1} K at 300 K is higher than the sum of the spin-only contribution (3.75 emu mol^{-1} K) for ten Cu^{II} atoms considering $g=2$ per formula unit. Upon cooling, the $\chi_M T$ product gradually increases to a maximum of 9.10 emu mol^{-1} K at 7 K, and then sharply decreases to 6.51 emu mol^{-1} K at 2 K. The magnetic susceptibility can be fitted to a Curie–Weiss with $C=4.97$ emu mol^{-1} K and $\theta=5.58$ K, in agreement with the presence of the dominant ferromagnetic exchange interactions among the Cu^{II} centers. A classical correlation between the experimental exchange constant and the Cu-O-Cu bond angle ϕ reveals that the complexes are generally antiferromagnetic for $\phi>98°$, but ferromagnetic for smaller angles.[27] Except for two pendant $[Cu(dap)(H_2O)_3]^{2+}$ ions, the Cu···Cu exchange interactions in **2** are mainly mediated through double μ-oxo bridges with the Cu-O-Cu bond ranging from 83.1 to 107.6°. Although there are some competitive antiferromagnetic and ferromagnetic interactions, the dominant ferromagnetic behavior is expectable since the most Cu-O-Cu angles are less than 98° within the Cu_8 core.

For compound **3**, the value of χ_M slowly increases from 0.11 emu mol^{-1} at 300 K to 0.32 emu mol^{-1} at 22 K, then exponentially to the maximum of 1.19 emu mol^{-1} at 2 K (Figure 7). The product of $\chi_M T$ decreases smoothly from 33.33 emu mol^{-1} K at 300 K to 2.38 emu mol^{-1} K at 2 K. The $\chi_M T$ value of 33.33 emu mol^{-1} K at 300 K is much lower than the expected value (57.0 emu mol^{-1} K) for a cluster of 12 noninteracting Fe^{III} ($S=5/2$) and 1.5 Fe^{II} ($S=2$) ions with $g=2.00$, indicating significant antiferromagnetic exchange interactions within the $Fe_{13.5}$ cores. In addition, the plot of χ_M^{-1} versus T in the range of 300–70 K is well described by the Curie–Weiss law with Curie constant $C=58.81$ emu mol^{-1} K and Weiss constant $\theta=-239.95$ K (Figure S11 in the Supporting Information), which further confirms the occurrence of strong antiferromagnetic exchange interactions between the Fe^{III} and Fe^{II} centers. Such a strong antiferromagnetic coupling has been observed in some iron–oxo clusters.[28]

The plots of χ_{mT} versus T and the best fit for **4** are displayed in Figure 8 in the range of 2–300 K, respectively. The value of $\chi_m T$ at 300 K is 2.33 emu mol^{-1} K, which is close to the spin only value of 2.25 emu mol^{-1} K expected for six uncoupled $S=1/2$ Cu^{II} centers considering $g=2$. When the system is cooled from 300 K to approximately 55 K, the $\chi_M T$ product is approximately constant with a slight decrease. Additionally, below 55 K, $\chi_M T$ product decreases abruptly with further lowering temperature reaching the minimum of 0.512 emu mol^{-1} K at 2 K. Moreover, the magnetic susceptibility data between 2 and 300 K are well described by the Curie–Weiss expression with Curie constant $C=2.42$ emu mol^{-1} K and Weiss constant $\theta=-3.52$ K (Fig-

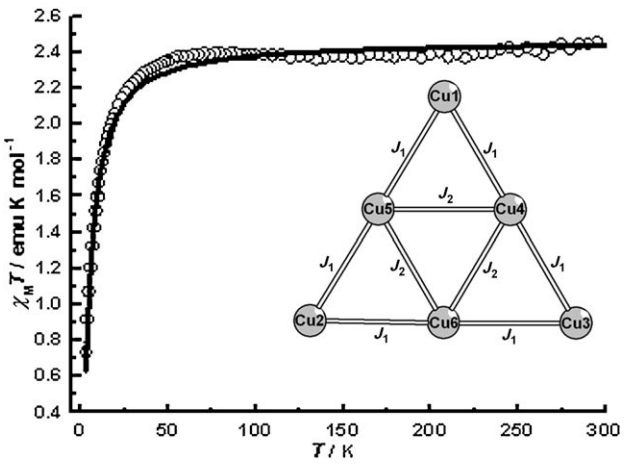

Figure 8. The plot of χ_{mT} versus T for for **4**. The solid line represents the best fit to experimental data. The inset illustrates the magnetic exchange pathways between adjacent metal ions.

ure S12 in the Supporting Information). This behavior is indicative of the presence of dominant antiferromagnetic interactions among the Cu^{II} centers. The appropriate Hamiltonian for Cu_6 system can be written as Equation (1) with $S_1 = S_2 = S_3 = S_4 = S_5 = S_6 = 1/2$ regardless of the second- and third-neighbor interactions between Cu^{II} ions with significantly long distances (more than 5.4 Å).

$$H = -2J_1(S_1S_4+S_1S_5+S_2S_5+S_2S_6+S_3S_4+S_3S_6) - 2J_2(S_4S_5+S_4S_6+S_5S_6) \quad (1)$$

The best-fitting parameters obtained with the MAGPACK package[29] are $J_1 = -3.31\ cm^{-1}$, $J_2 = -0.67\ cm^{-1}$, $g = 2.10$, and the agreement factor $R = 3.39 \times 10^{-4}$, which proves the antiferromagnetic coupling interactions among the Cu^{II} ions. For **4**, the exchange pathway between each pair Cu^{II} ions are transmitted through one μ-oxo and one μ-O(H) bridge, with the Cu-O-Cu bond angles of about 90° (89.8–94.5°) and 100° (100.7–104.7°). In this competitive environment, the antiferromagnetic interactions tend to dominate in many O-bridged Cu^{II} complexes.[27b,c]

Since **5**–**8** contain the similar Ni_6 core, only **5** was selected as a model for magnetic characterization. For **5**, the plots of $\chi_M T$ versus T and the best fit are shown in Figure 9 under a constant magnetic field of 5 kOe. The value of $\chi_M T$ at 300 K is 8.25 emu mol^{-1} K, typical values for six noncorrelated Ni^{II} ion with $g > 2.00$.[30] Upon cooling, $\chi_M T$ increases to a maximum of 21.63 emu mol^{-1} K at 11 K. This magnetic behavior typifies the ferromagnetic coupling interactions between adjacent Ni^{II} centers. A sudden decrease of $\chi_M T$ value below 11 K suggests the presence of the significant ZFS effects in the ground state. Note that the observation that $\chi_M T$ is less field-dependent for applied fields below 5 kOe precludes the presence of significant intermolecular interactions.[31] The best fit of the Curie–Weiss law on the correlation between the inverse magnetic susceptibility χ_M^{-1} and temperature T in the range of 30–300 K yields the Curie constant $C = 7.59$ emu K mol^{-1} and Weiss constant $\theta = 22.07$ K (Figure S13 in the Supporting Information), indicating the ferromagnetic exchange interactions. As the temperature decreases from 50 to 2 K, the Curie–Weiss law is not followed, possibly resulting from the presence of ZFS effect. A theoretical analysis of the magnetic behavior of **5** was performed by using the isotropic Heisenberg exchange Hamiltonian taking into account the ZFS effects, but not the second- and third-neighbor interactions, which are negligible, between Ni^{II} ions with significantly long distances (more than 5.4 Å), as in this way analytical expressions for the eigenvalues and susceptibilities are easily derived from the vector coupling method of Kambé.[32] The appropriate Hamiltonian for the Ni_6 system with the isotropic model can be written as Equation (2) with $S_1 = S_2 = S_3 = S_4 = S_5 = S_6 = 1$.

$$H = -2J_1(S_1S_4+S_1S_5+S_2S_5+S_2S_6+S_3S_4+S_3S_6) - 2J_2(S_4S_5+S_4S_6+S_5S_6) + \sum DS_{iZ}^2 \quad (2)$$

In Equation (2), J_1 is the exchange constant between Ni^{II} ions situated in the corners of equilateral triangle and Ni^{II} ions sitting on the edge midpoint of equilateral triangle, J_2 is the exchange constant between Ni^{II} ions sitting on the edge midpoint of equilateral triangle, and D represents the ZFS parameter. Calculations were performed with the MAGPACK package.[29] An excellent agreement with the experimental data was obtained with the following set of parameters: $J_1 = 0.63\ cm^{-1}$, $J_2 = 1.10\ cm^{-1}$, $g = 2.14$, $D = 1.00\ cm^{-1}$, and the agreement factor $R = 2.50 \times 10^{-4}$, which confirms the ferromagnetic coupling interactions among the Ni^{II} centers.

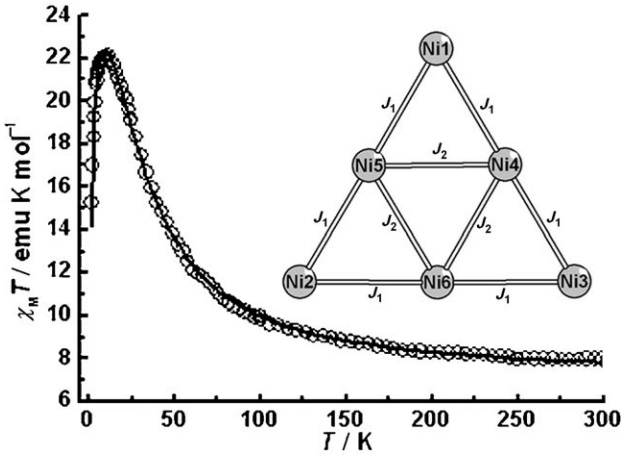

Figure 9. The plot of χ_{mT} versus T for **5**. The solid line represents the best fit to experimental data. The inset illustrates the magnetic exchange pathways between adjacent metal ions.

Thermogravimatric analysis: The thermogravimatric behavior of compounds **1**–**8** was investigated (Figure S4 in the Supporting Information). The TG curve of **1** shows two steps of weight loss in the range of 30–800 °C. The first weight loss is 4.41 % from 30–301 °C, assigned to the release of 4.5 lattice water and ten coordinated water molecules (calcd 4.06 %), followed by the loss of 12.17 % corresponding to the removal of eight dap ligands and the dehydration of six hydroxyl groups (calcd 11.32 %) from 301–800 °C. The weight loss process of **2** is divided into two steps in the range of 30–800 °C. The weight loss of 3.95 % during the first step from 30–243 °C corresponds to the release of six lattice water and six coordinated water molecules (calcd 3.72 %). On further heating, the second weight loss of 8.30 % between 243–800 °C is approximately attributed to the removal of two coordinated water molecules and six dap ligands (calcd 9.16 %). Because of amphibolous limits between adjacent steps of weight loss, the TG curve of **3** can be viewed as one slow-step process with the total weight loss of 22.98 % from 30–800 °C, corresponding to the removal of 130 lattice water molecules and three protonated en molecules and the dehydration of 12 hydroxyl groups and 15 protons (calcd 22.06 %). The TG curve of **4** indicates two weight-loss steps. The first weight loss of 4.14 % (calcd 4.17 %) between 30–103 °C corresponds to the release of

seven lattice water molecules. After 103 °C, a gradual weight loss of 8.20 % (calcd 8.65 %) until 800 °C is observed and assigned to the removal of three coordinated water molecules, three en molecules, and the dehydration of three hydroxyl groups. Because their structural similarities, the weigh loss behaviors of **5**–**8** are very similar and show three weight-loss steps with amphibolous limits, therefore, it can be regarded as one gradual weight loss. For **5**, the total weight loss of 12.64 % from 30–800 °C corresponds to the removal of seven lattice water molecules, six coordinated water molecules, three en ligands, and the dehydration of three hydroxyl groups per formula unit (calcd 12.94 %). For **6**, the total weight loss of 13.30 % in the range of 30–800 °C is in good agreement with the theoretical value of 13.81 %, attributable to loss of seven lattice water molecules, eight coordinated water molecules, two en ligands, and the dehydration of three hydroxyl groups per formula unit. For **7**, the gradual weight loss is 15.66 % between 30 and 800 °C, approximately assigned to the release of seven lattice water molecules, eight coordinated water molecules, two dap ligands, and the dehydration of three hydroxyl groups per formula unit (calcd 14.60 %), respectively. For **8**, it starts to lose weight in a broad temperature range, and by 800 °C it loses about 15.08 % of its weight, approximately agreeing with the calculated 14.29 % for the removal of 3.5 lattice water molecules, six coordinated water molecules, four en ligands, and the dehydration of three hydroxyl groups per formula unit. These observations indicate the experimental values are in approximately consistence with the theoretical values.

Conclusion

A series of novel TMSPs, from single cluster to poly(POM) species, one-dimensional chain and three-dimensional frameworks based on trivacant Keggin α-XW_9 precursors and in situ-generated TM clusters, have been successfully made under hydrothermal conditions. The strategy is based on the consideration that the lacunary sites of α-XW_9 fragments may act as the structure-directing agents and induce the formation of TM clusters or large oligomers of TM clusters. They have been structurally characterized by elemental analyses, IR spectra, diffuse reflectance spectra, thermogravimatric analysis, and single-crystal X-ray crystallography. Compound **1** not only is an unique example of the heptanuclear TMC-substituted polyoxotungstate based on single trivacant Keggin fragment, but it also incorporates the highest number of 3d TM cations in any other reported trivacant Keggin or Dawson polyoxotungstate monomers to date. Compound **2** represents an unprecedented octa-TM cluster encapsulated dimeric POM, while **3** is a Fe_4O_4-cubane-containing tetramer of trivacant Keggin POM. Notably, compound **4** represents an unprecedented three-dimensional framework with hexagonal channels enclosed by three interweaved helical chains in the TMSP chemistry. The common feature of **5**–**8** is that they are composed of a B-α-isomeric trivacant Keggin fragment capped by a hexa-Ni^{II} cluster. The reflectance spectrum measurements reveal that these compounds may be potential semiconductor materials. The magnetic properties of **1**–**5** were investigated and the magnetic behaviors of **4** and **5** were theoretically simulated by the MAGPACK magnetic program package.

The key points of the synthetic procedures on TMSPs under hydrothermal conditions have been well established.[6a]

1) The molar ratio of lacunary POM precursors/TM ions significantly influences the nuclearity number of TM clusters generated in situ and the structural diversity of TMSP products.
2) The nature of different lacunary POM precursors can also tune the nuclearity number of TM clusters generated in situ.
3) The nature of TM ions determines their activity to react lacunary POM precursors.
4) The control of temperature can tune the formation of different TMSP phases.
5) The size and shape of organoamines can influence their activity and chelating capability as well as determine whether they can work as structure-stabilizing agents to enhance the stability of TMSP products.

These key factors not only provide us with a useful and important guide to the synthesis of TMSPs, but they also indicate that hydrothermal techniques can offer an effective way for making both lacunary POMs and poly(POM) species that incorporate high-nuclear TM clusters. In addition, the trivacant sites of the α-XW_9 fragment can act as the structure-directing agents that firstly capture a trimeric metal cluster to complete the Keggin-type POM cluster and then further aggregate to form high-nuclear TMSPs. Further work is in progress to prepare other new TMSPs built from larger metal cluster aggregates and other types of lacunary precursors (divacant and multivacant POM fragments) or mixed multilacunary precursors under hydrothermal conditions.[34] In addition to trivacant Keggin POM precursors, we are also investigating such reaction systems with monovacant Keggin/Dawson POM and tri-/hexavacant Dawson POM precursors; this work is in progress and will be reported in due time. The successful preparation of the above new TMSPs indicate that the combination chemistry between lacunary POM precursors and the transition metal clusters generated in situ can be realized under rational hydrothermal conditions. In a word, it is reasonable to believe that the present work will be important in expanding the study of POM-based materials.

Experimental Section

Chemicals, reagents, and analyses: All chemicals were used as purchased without purification. The lacunary precursors $Na_9[A\text{-}\alpha\text{-}PW_9O_{34}]\cdot 7H_2O$[4d] and $K_{10}[A\text{-}\alpha\text{-}SiW_9O_{34}]\cdot 25H_2O$[4f] were synthesized as previously described. Elemental analyses (C, H, and N) were performed on a

PE 2400 II elemental analyzer. Inductively coupled plasma (ICP) analysis was performed on a Jobin Yvon ultima2 spectrometer. Energy-dispersive X-ray analysis (EDXA) was taken by using a JEOL-JSM-6700F field-emission scanning electron microscope. X-ray photoelectron spectroscopy (XPS) was recorded on an Axis Ultra X-ray photoelectron spectrometer and the XPS analysis was corrected with reference to C1s (284.6 eV). The IR spectra were obtained on an ABB Bomen MB 102 spectrometer in the range of 4000–400 cm^{-1} with pressed KBr pellets. Thermogravimetric analyses (TGA) were performed on a Mettler TGA/SDTA851 thermal analyzer under an air-flow atmosphere with a heating rate of 10 °C min^{-1} in the temperature region of 30–1000 °C. Variable-temperature magnetic susceptibility measurements were carried out in the temperature range of 2–300 K with a Quantum Design MPMS-5 magnetometer. Experimental susceptibilities were corrected for diamagnetism of the constituent atoms by use of Pascal's constants.

Table 1. Crystallographic data and structure refinements for **1**–**8**.

	1	**2**	**3**	**4**
formula	$C_{24}N_{16}H_{123}O_{94.5}P_2Ni_{14}W_{18}$	$C_{18}H_{88}N_{12}O_{82}Cu_{10}Si_2W_{18}$	$C_6N_6H_{317}O_{294}Fe_{13.5}P_8W_{36}$	$C_6N_6H_{47}O_{47}PCu_6W_9$
M_r	6341.56	5785.88	12799.38	3022.33
crystal system	triclinic	monoclinic	monoclinic	hexagonal
space group	$P\bar{1}$	$P2_1/c$	$C2/m$	$P6_3$
a [Å]	17.5015(6)	13.2517(6)	36.786(12)	13.3026(16)
b [Å]	17.9867(5)	16.1610(7)	25.742(12)	13.3026(16)
c [Å]	19.8580(5)	23.6199(11)	21.592(9)	16.752(3)
α [°]	82.651(6)	90	90	90
β [°]	82.124(6)	98.892(2)	95.350(13)	90
γ [°]	80.313(5)	90	90	120
V [Å^3]	6068.6(3)	4997.7(4)	20357(14)	2567.3(6)
crystal size [mm^3]	0.11×0.10×0.08	0.20×0.12×0.05	0.15×0.15×0.10	0.22×0.20×0.16
index range	$-20\le h\le 20$	$-13\le h\le 15$	$-37\le h\le 43$	$-15\le h\le 17$
	$-19\le k\le 21$	$-19\le k\le 19$	$-30\le k\le 30$	$-17\le k\le 15$
	$-22\le l\le 23$	$-28\le l\le 25$	$-25\le l\le 25$	$-21\le l\le 21$
measured reflns	38286	30591	63921	19742
unique reflns	21042	8634	18173	3826
R_{int}	0.0386	0.0369	0.0782	0.0406
Z	2	2	4	2
λ [Å]	0.71073	0.71073	0.71073	0.71073
μ [mm^{-1}]	19.225	22.826	21.346	22.642
GOF on F^2	1.093	1.081	1.097	0.934
R_1[a] $[I>2\sigma(I)]$	0.0578	0.0356	0.0755	0.0185
wR_2[b] $[I>2\sigma(I)]$	0.1303	0.0838	0.1860	0.0364
R_1[a] (all data)	0.0775	0.0404	0.0928	0.0219
wR_2[b] (all data)	0.1419	0.0865	0.1981	0.0370

	5	**6**	**7**	**8**
formula	$C_6N_6H_{53}O_{50}PNi_6W_9$	$C_4N_4H_{49}O_{52}PNi_6W_9$	$C_6N_4H_{53}O_{52}PNi_6W_9$	$C_8N_8H_{54}O_{46.5}SiNi_{6.5}W_9$
M_r	3047.42	3023.35	3051.40	3070.95
crystal system	monoclinic	monoclinic	monoclinic	monoclinic
space group	$P2_1/n$	$P2_1/n$	$P2_1/n$	$P2_1/n$
a [Å]	13.430(2)	13.5930(15)	13.872(3)	12.926(3)
b [Å]	19.100(3)	18.772(2)	18.845(4)	23.534(6)
c [Å]	21.650(3)	19.300(2)	19.452(4)	17.003(4)
α [°]	90	90	90	90
β [°]	102.490(3)	92.762(2)	91.465(2)	102.132(4)
γ [°]	90	90	90	90
V [Å^3]	5422.1(14)	4919.0(10)	5083.7(17)	5057(2)
crystal size [mm^3]	0.22×0.20×0.16	0.16×0.08×0.04	0.10×0.10×0.05	0.15×0.06×0.03
index range	$-15\le h\le 17$	$-16\le h\le 15$	$-18\le h\le 12$	$-16\le h\le 16$
	$-24\le k\le 22$	$-23\le k\le 23$	$-24\le k\le 24$	$-29\le k\le 30$
	$-28\le l\le 23$	$-23\le l\le 23$	$-25\le l\le 24$	$-17\le l\le 22$
measured reflns	41904	33541	38832	39349
unique reflns	12312	9544	11497	11536
R_{int}		0.0520	0.0345	0.0532
Z	4	4	4	4
λ [Å]	0.71073	0.71073	0.71073	0.71073
μ [mm^{-1}]	21.178	23.344	22.590	22.877
GOF on F^2	1.039	1.039	1.096	1.081
R_1[a] $[I>2\sigma(I)]$	0.0360	0.0253	0.0454	0.0454
wR_2[b] $[I>2\sigma(I)]$	0.0863	0.0601	0.1028	0.0916
R_1[a] (all data)	0.0428	0.0286	0.0538	0.0582
wR_2[b] (all data)	0.0904	0.0617	0.1076	0.0987

[a] $R_1=\Sigma||F_o|-|F_c||/\Sigma|F_o|$. [b] $wR_2=[\Sigma w(F_o^2-F_c^2)^2/\Sigma w(F_o^2)^2]^{1/2}$; $w=1/[\sigma^2(F_o^2)+(xP)^2+yP]$, $P=(F_o^2+2F_c^2)/3$, in which $x=0.0642$, $y=63.6140$ for **1**, $x=0.0419$, $y=45.9708$ for **2**, $x=0.0976$, $y=886.3510$ for **3**, $x=0.0483$, $y=0.0000$ for **4**, $x=0.0483$, $y=0.0000$ for **5**, $x=0.0372$, $y=0$ for **6**, $x=0.0555$, $y=0$ for **7**, $x=0.0400$, $y=0$ for **8**.

$[Ni_6(dap)_3PW_9][Ni_7(dap)_3PW_9]$ (1): A mixture of $Na_9[A\text{-}\alpha\text{-}PW_9O_{34}]\cdot 7H_2O$ (0.369 g, 0.141 mmol), $NiCl_2\cdot 6H_2O$ (0.237 g, 1.000 mmol), dap (0.20 mL, 2.356 mmol), and H_2O (8 mL, 444 mmol) was stirred for 4 h, sealed in a 20 mL Teflon-lined steel autoclave, heated at 160 °C for 5 days, and then cooled to room temperature. Green prismatic crystals were obtained by filtration; they were washed with distilled water and dried in air. Yield: ~40 % (based on $Na_9[A\text{-}\alpha\text{-}PW_9O_{34}]\cdot 7H_2O$); elemental analysis (%) calcd for $C_{24}N_{16}H_{123}O_{94.5}P_2Ni_{14}W_{18}$: C 4.55, H 1.96, N 3.53; found: C 4.44, H 2.03, N 3.21; IR (KBr pellet): $\tilde{\nu}$ = 3455, 3354, 3286, 2968, 1603, 1462, 1390, 1354, 1039, 939, 847, 798, 717, 508 cm^{-1}.

$[Cu_8(dap)_4(SiW_9)_2]$ (2): A mixture of $K_{10}[A\text{-}\alpha\text{-}SiW_9O_{34}]\cdot 25H_2O$ (0.297 g, 0.097 mmol), $CuCl_2\cdot 2H_2O$ (0.128 g, 0.750 mmol), dap (0.05 mL, 0.589 mmol), and H_2O (5 mL, 278 mmol) was heated at 100 °C for 5 days. Dark green crystals were isolated. Yield: ~33 %; elemental analysis (%) calcd for $C_{18}H_{88}N_{12}O_{82}Cu_{10}Si_2W_{18}$: C 3.74, H 1.53, N 2.91; found: C 3.65, H 1.78, N 2.84; IR (KBr pellet): $\tilde{\nu}$ = 3431, 3286, 3221, 2968, 2931, 2880, 1627, 1567, 1458, 1386, 1056, 1024, 947, 879, 722, 505 ppm.

$[Fe_{13.5}(PW_9)_4]$ (3): A mixture of $Na_9[A\text{-}\alpha\text{-}PW_9O_{34}]\cdot 7H_2O$ (0.246 g, 0.094 mmol), $FeSO_4\cdot 7H_2O$ (0.139 g, 0.500 mmol), en (0.05 mL, 0.740 mmol), HAc (0.10 mL, 1.748 mmol), and H_2O (5 mL, 278 mmol) were heated together at 80 °C for 5 days. The brown red prism crystals were harvested. Yield: ~45 %; elemental analysis (%) calcd for $C_6N_6H_{317}O_{294}Fe_{13.5}P_8W_{36}$: C 0.56, H 2.50, N 0.66, P 1.94, Fe 5.89, W 51.71; found: C 0.70, H 2.80, N 0.72, P 2.04, Fe 5.69, W 53.56. The P:Fe:W ratio obtained by EDXA are in agreement with the formula of $[Fe_{13.5}(PW_9)_4]$ obtained from the structure refinement (obsd P:Fe:W = 1:1.61:4.59, calcd P:Fe:W = 1:1.69:4.50). In addition, the ICP and EDXA show that there is no Na in the structure of **3**. IR (KBr pellet): $\tilde{\nu}$ = 3443, 1607, 1503, 1446, 1386, 1350, 1052, 967, 947, 867, 786, 726, 702, 476 cm^{-1}.

$[Cu_6(en)_3PW_9]$ (4): The procedure for the formation of compound **3** was employed, but instead of $FeSO_4\cdot 7H_2O$ we used $CuCl_2\cdot 2H_2O$ (0.170 g, 1.00 mmol). Yield: ~34 %; elemental analysis (%) calcd for $C_6N_6H_{47}O_{47}PCu_6W_9$: C 2.38, H 1.57, N 2.78; found: C 2.32, H 1.60, N 2.59; IR (KBr pellet): $\tilde{\nu}$ = 3426, 3330, 3253, 2956, 1603, 1458, 1394, 1354, 1124, 1060, 1024, 951, 935, 875, 839, 798, 730, 589, 484 cm^{-1}.

$[Ni_6(en)_3PW_9]$ (5): $Na_9[A\text{-}\alpha\text{-}PW_9O_{34}]\cdot 7H_2O$ (0.123 g, 0.047 mmol), $NiCl_2\cdot 6H_2O$ (0.237 g, 1.000 mmol), en (0.05 mL, 0.740 mmol), and glacial acetic acid (HAc) (0.05 mL, 0.874 mmol) were successively dissolved in H_2O (5 mL, 277 mmol); the mixture was then stirred for 4 h, sealed in a 20 mL Teflon-lined steel autoclave, heated at 80 °C for 5 days, and then cooled to room temperature. Green prismatic crystals were obtained by filtration; they were washed with distilled water and dried in air. Yield: ~64 %; elemental analysis (%) calcd for $C_6N_6H_{53}O_{50}PNi_6W_9$: C 2.36, H 1.53, N 2.76; found: C 2.22, H 1.85, N 2.55; IR (KBr pellet): $\tilde{\nu}$ = 3478, 3342, 3286, 1623, 1583, 1104, 1035, 943, 842, 798, 713, 508 cm^{-1}.

$[Ni_6(en)_2PW_9]$ (6): The procedure for the formation of compound **5** was employed, but the temperature was elevated to 130 °C. Yield: ~60 %; elemental analysis (%) calcd for $C_4N_4H_{49}O_{52}PNi_6W_9$: C 1.59, H 1.63, N 1.85; found: C 1.61, H 1.73, N 1.71; IR (KBr pellet): $\tilde{\nu}$ = 3487, 3350, 3286, 1623, 1583, 1112, 1036, 943, 846, 798, 714, 504 cm^{-1}.

$[Ni_6(dap)_2PW_9]$ (7): The procedure for the formation of compound **5** was employed, but en was replaced with dap (0.05 mL, 0.589 mmol). Yield: ~43 %; elemental analysis (%) calcd for $C_6N_4H_{53}O_{52}PNi_6W_9$: C 2.36, H 1.75, N 1.84; found: C 2.24, H 1.81, N 1.73; IR (KBr pellet): $\tilde{\nu}$ = 3455, 3350, 3286, 1603, 1039, 939, 850, 798, 718, 508 cm^{-1}.

$[Ni_6(en)_3SiW_9]$ (8): The procedure for the formation of compound **5** was employed, but with $K_{10}[A\text{-}\alpha\text{-}SiW_9O_{34}]\cdot 25H_2O$ (0.246 g, 0.080 mmol), $NiCl_2\cdot 6H_2O$ (0.237 g, 1.000 mmol), en (0.10 mL, 1.480 mmol), HAc (0.05 mL, 0.874 mmol) and H_2O (8 mL, 444 mmol). Yield: ~52 %; elemental analysis (%) calcd for $C_8N_8H_{54}O_{46.5}SiNi_{6.5}W_9$: C 3.13, H 1.77, N 3.65; found: C 2.69, H 1.91, N 3.22; IR (KBr pellet): $\tilde{\nu}$ = 3584, 3431, 3350, 3274, 2931, 2887, 1599, 1458, 1386, 1354, 1277, 1233, 1132, 1104, 1040, 939, 875, 826, 778, 710, 541, 508 cm^{-1}.

X-ray crystallography: Intensity data were collected at 293 K with a RIGAKU Saturn 70 CCD diffractometer for **1**, **4**, **5**, **6**, and **8**, and a RIGAKU Mercury CCD/AFC diffractometer for **2**, **3** and **7** using graphite-monochromated $Mo_{K\alpha}$ radiation (λ = 0.71073 Å), respectively. Routine Lorentz and polarization corrections were applied. The absorption correction was based on multiple and symmetry-equivalent reflections in the data set by using the SADABS program. The structures were solved by direct methods and refined by full-matrix least-squares methods on F^2 with the SHELXTL-97 program package.[35] No hydrogen atoms associated with the water molecules were located from the difference Fourier map. Positions of the hydrogen atoms attached to the carbon and nitrogen atoms were geometrically placed. All hydrogen atoms were refined isotropically as a riding mode using the default SHELXTL parameters. For **1**, the Ni7 atom was disordered over two positions with the occupation factors of 0.7 and 0.3, respectively. For **3**, the occupation factors of Fe8, Fe9, and Fe10 were determined as 0.25 according to the results of inductively coupled plasma and energy-dispersive X-ray analysis. In addition, P4, P5, and P6 were set to be disordered in order to decrease the size of the residual electron peaks. For **1**–**8**, all non-hydrogen atoms were refined anisotropically except for some carbon atoms and water molecules. Crystallographic data and structure refinements for **1**–**8** are given in Table 1. CCDC 624225 (**1**), 641518 (**2**), 624226 (**3**), 624227 (**4**), 624221 (**5**), 624222 (**6**), 624223 (**7**) and 624224 (**8**) contain the supplementary crystallographic data for this paper. These data can be obtained free of charge from The Cambridge Crystallographic Data Centre via www.ccdc.cam.ac.uk/data_request/cif.

Acknowledgements

This work was supported by the National Natural Science Fund for Distinguished Young Scholars of China (grant 20725101), the 973 Program (grant 2006CB932904), the NNSF of China (grant 20473093), the NSF of Fujian Province (grant E0510030 and 2004J043), and the Knowledge Innovation Program of the Chinese Academy of Sciences.

[1] a) *Polyoxometalates: From Platonic Solids to Anti Retroviral Activity* (Eds.: M. T. Pope, A. Müller), Kluwer, Dordrecht, **1994**; b) Special issue on polyoxometalates: *Chem. Rev.* **1998**, *98*, 1; c) *Polyoxometalate Chemistry: From Topology via Self-Assembly to Applications* (Eds.: M. T. Pope, A. Müller), Kluwer, Dordrecht, **2001**; d) K. Kamata, K. Yonehara, Y. Sumida, K. Yamaguchi, S. Hikichi, N. Mizuno, *Science* **2003**, *300*, 964; e) T. M. Anderson, W. A. Neiwert, M. L. Kirk, P. M. B. Piccoli, A. J. Schultz, T. F. Koetzle, D. G. Musaev, K. Morokuma, R. Cao, C. L. Hill, *Science* **2004**, *306*, 2074; f) D.-L. Long, H. Abbas, P. Kögerler, L. Cronin, *J. Am. Chem. Soc.* **2004**, *126*, 13880; g) X. Fang, T. M. Anderson, C. Benelli, C. L. Hill, *Chem. Eur. J.* **2005**, *11*, 712.

[2] a) T. J. R. Weakley, H. T. Evans, Jr., J. S. Showell, G. F. Tourné, C. M. Tourné, *J. Chem. Soc. Chem. Commun.* **1973**, 139; b) N. Casañ-Pastor, J. Bas-Serra, E. Coronado, G. Pourroy, L. C. W. Baker, *J. Am. Chem. Soc.* **1992**, *114*, 10380; c) F. Xin, M. T. Pope, *J. Am. Chem. Soc.* **1996**, *118*, 7731; d) M. Bösing, A. Nöh, I. Loose, B. Krebs, *J. Am. Chem. Soc.* **1998**, *120*, 7252; e) J. M. Clemente-Juan, E. Coronado, J. R. Galán-Mascarós, C. J. Gómez-García, *Inorg. Chem.* **1999**, *38*, 55; f) B. S. Bassil, S. Nellutla, U. Kortz, A. C. Stowe, J. van Tol, N. S. Dalal, B. Keita, L. Nadjo, *Inorg. Chem.* **2005**, *44*, 2659.

[3] a) M. Hölscher, U. Englert, B. Zibrowius, W. F. Hölderich, *Angew. Chem.* **1994**, *106*, 2552; *Angew. Chem. Int. Ed. Engl.* **1994**, *33*, 2491; b) M. Nyman, F. Bonhomme, T. M. Alam, M. A. Rodriguez, B. R. Cherry, J. L. Krumhansl, T. N. Nenoff, A. M. Sattler, *Science* **2002**, *297*, 996; c) M. Nyman, F. Bonhomme, T. M. Alam, J. B. Parise, G. M. B. Vaughan, *Angew. Chem.* **2004**, *116*, 2847; *Angew. Chem. Int. Ed.* **2004**, *43*, 2787; d) A. Dolbecq, P. Mialane, L. Lisnard, J. Marrot, F. Sécheresse, *Chem. Eur. J.* **2003**, *9*, 2914; e) B. Yan, Y. Xu, X. Bu, N. K. Goh, L. S. Chia, G. D. Stucky, *J. Chem. Soc. Dalton Trans.* **2001**, 2009; f) Z. Hang, Y. Zhao, J. Peng, H. Ma, Q. Liu, E. Wang, N. Hu, H. Jia, *Eur. J. Inorg. Chem.* **2005**, 264; g) C.-M. Wang, S.-T. Zheng, G.-Y. Yang, *Inorg. Chem.* **2007**, *46*, 616.

[4] a) A. Tézé, G. Hervé, *Inorg. Synth.* **1990**, *27*, 85; b) R. Contant, *Inorg. Synth.* **1990**, *27*, 104; c) N. Haraguchi, Y. Okaue, T. Isobe, Y. Matsuda, *Inorg. Chem.* **1994**, *33*, 1015; d) P. J. Domaille, *Inorg. Synth.* **1990**, *27*, 96; e) N. H. Nsouli, B. S. Bassil, M. H. Dickman, U. Kortz, B. Keita, L. Nadjo, *Inorg. Chem.* **2006**, *45*, 3858; f) G. Hervé, A. Tézé, *Inorg. Chem.* **1977**, *16*, 2115; g) M. Bösing, I. Loose, H. Pohlmann, B. Krebs, *Chem. Eur. J.* **1997**, *3*, 1232.

[5] a) R. A. Laudise, *Prog. Inorg. Chem* **1962**, *3*, 1–47; b) A. Rabenau, *Angew. Chem.* **1985**, *97*, 1017; *Angew. Chem. Int. Ed. Engl.* **1985**, *24*, 1026; c) R. A. Laudise, *Chem. Eng. News* **1987**, *65*, 30; d) P. J. Hagrman, D. Hagrman, J. Zubietua, *Angew. Chem.* **1999**, *111*, 2798; *Angew. Chem. Int. Ed.* **1999**, *38*, 2638; e) J. Gopalakrishnan, *Chem. Mater.* **1995**, *7*, 1265; f) D. Hagrman, C. Sangregorio, C. J. O'Connor, J. Zubieta, *J. Chem. Soc. Dalton Trans.* **1998**, 3707; g) H. Jin, Y. Qi, E. Wang, Y. Li, C. Qin, X. Wang, S. Chang, *Eur. J. Inorg. Chem.* **2006**, 4541.

[6] a) S.-T. Zheng, D.-Q. Yuan, H.-P. Jia, J. Zhang, G.-Y. Yang, *Chem. Commun.* **2007**, 1858; b) J.-W. Zhao, B. Li, S.-T. Zheng, G.-Y. Yang, *Cryst. Growth Des.* **2007**, accepted for publication, DOI: 10.1021/cg070783b; c) S.-T. Zheng, D.-Q. Yuan, J. Zhang, G.-Y. Yang, *Inorg. Chem.* **2007**, *46*, 4569; d) J.-W. Zhao, S.-T. Zheng, G.-Y. Yang, *J. Solid State Chem.* **2007**, published online, DOI:10.1016/j.jssc.2007.09.029; e) S.-T. Zheng, M.-H. Wang, G.-Y. Yang, *Chem. Asian J.* **2007**, *2*, 1380; f) $[Ni(en)_2]_{0.5}[\{Ni_6(\mu_3\text{-}OH)_3(en)_3(H_2O)_6\}(B\text{-}\alpha\text{-}GeW_9O_{34})]\cdot 3H_2O$: monoclinic, $P2_1n$, $a=12.9432(3)$, $b=23.5840(5)$, $c=17.0394(4)$ Å, $\beta=102.17°$, $V=5084.4(2)$ Å^3; $[Ni_6(dap)_3(H_2O)_6(OH)_3][B\text{-}\alpha\text{-}GeW_9O_{34}]\cdot H_3O\cdot 4H_2O$: monoclinic, $P2_1/c$, $a=13.919(16)$, $b=23.73(3)$, $c=18.815(16)$ Å, $\beta=115.77(6)°$, $V=5596(11)$ Å^3; g) $H_4[Cu_8(dap)_4(H_2O)_2(B\text{-}\alpha\text{-}GeW_9O_{34})_2]\cdot 13H_2O$: monoclinic, $P2_1/c$, $a=13.24380(10)$, $b=16.5562(2)$, $c=23.6087(1)$ Å, $\beta=98.6960(10)°$, $V=5117.10(8)$ Å^3.

[7] a) W. H. Knoth, P. J. Domaille, R. L. Harlow. *Inorg. Chem.* **1986**, *25*, 1577; b) C. R. Mayer, R. Thouvenot, *J. Chem. Soc. Dalton Trans.* **1998**, 7; c) U. Kortz, I. M. Mbomekalle, B. Keita, L. Nadjo, P. Berthet, *Inorg. Chem.* **2002**, *41*, 6412.

[8] a) W. M. Wesley, W. G. H. Harry, *Reflectance Spectroscopy*, Wiley, New York, **1966**, pp. 104–169; b) J. I. Pankove, *Optical Processes in Semiconductors*, Prentice–Hall, Englewood Cliffs, NJ, **1997**, pp. 34–86; c) Y. Xia, P. Wu, Y. Wei, Y. Wang, H. Guo, *Cryst. Growth Des.* **2006**, *6*, 253; d) L. Zhang, Y. Wei, C. Wang, H. Guo, P. Wang, *J. Solid State Chem.* **2004**, *177*, 3433; e) J. Liao, J. Juang, Y. Lai, *Cryst. Growth Des.* **2006**, *6*, 354; f) Q. G. Zhai, X. Y. Wu, S. M. Chen, Z. G. Zhao, C. Z. Lu, *Inorg. Chem.* **2007**, *46*, 5046.

[9] a) R. G. Finke, M. W. Droege, P. J. Domialle, *Inorg. Chem.* **1987**, *26*, 3886; b) X. Zhang, Q. Chen, D. C. Duncan, R. J. Lachicotte, C. L. Hill, *Inorg. Chem.* **1997**, *36*, 4381.

[10] A. Müller, F. Peters, M. T. Pope, D. Gatteschi, *Chem. Rev.* **1998**, *98*, 239, and references therein.

[11] a) I. D. Brown, D. Altermatt, *Acta Crystallogr. Sect. B* **1985**, *41*, 244; b) In the reaction system of **3**, the Fe^{III} cations are formed from the oxidation of Fe^{II} cations. To determine the chemical formula of **3**, BVS calculations were carried out.[11a] The oxidation states of ions Fe1–Fe10 are 2.94, 3.15, 3.19, 3.10, 3.05, 3.08, 3.09, 2.25, 2.14, and 2.28, respectively. The oxidation states of the W1–W19 atoms are 6.09, 6.37, 5.92, 6.21, 6.35, 6.10, 6.06, 6.08, 6.09, 6.29, 6.15, 6.21, 6.16, 6.07, 6.11, 6.33, 6.02, 6.15, and 6.19. From the above analysis, the oxidation states of all the W atoms are +6, while the oxidation states of Fe1–Fe7 included in the trivacant sites of four B-α-PW_9 fragments are +3, and the oxidation states of Fe8-Fe10 atoms included in the central Fe_4O_4 core are +2.

[12] U. Kortz, A. Tézé, G. Hervé, *Inorg. Chem.* **1999**, *38*, 2038.

[13] P. Mialane, A. Dolbecq, J. Marrot, E Rivière, F. Sécheresse, *Angew. Chem.* **2003**, *115*, 3647; *Angew. Chem. Int. Ed.* **2003**, *42*, 3523.

[14] G.-S. Kim, H. Zeng, D. VanDerveer, C. L. Hill, *Angew. Chem.* **1999**, *111*, 3413; *Angew. Chem. Int. Ed.* **1999**, *38*, 3205.

[15] R. C. Howell, F. G. Perez, S. Jain, W. D. Horrocks, Jr., A. L. Rheingold, L. C. Francesconi, *Angew. Chem.* **2001**, *113*, 4155; *Angew. Chem. Int. Ed.* **2001**, *40*, 4031.

[16] U. Kortz, S. S. Hamzeh, N. A. Nasser, *Chem. Eur. J.* **2003**, *9*, 2945.

[17] a) F. Hussain, B. S. Bassil, L. Bi, M. Reicke, U. Kortz, *Angew. Chem.* **2004**, *116*, 3567; *Angew. Chem. Int. Ed.* **2004**, *43*, 3485; b) U. Kortz, F. Hussain, M. Reicke, *Angew. Chem.* **2005**, *117*, 3839; *Angew. Chem. Int. Ed.* **2005**, *44*, 3773; c) S. S. Mal, U. Kortz, *Angew. Chem.* **2005**, *117*, 3843; *Angew. Chem. Int. Ed.* **2005**, *44*, 3777.

[18] a) B. Godin, Y. Chen, J. Vaissermann, L. Ruhlmann, M. Verdaguer, P. Gouzerh, *Angew. Chem.* **2005**, *117*, 3132; *Angew. Chem. Int. Ed.* **2005**, *44*, 3072; b) C. P. Pradeep, D. L. Long, P. Kögerler, L. Cronin, *Chem. Commun.* **2007**, 4254.

[19] K. Wassermann, M. H. Dickman, M. T. Pope, *Angew. Chem.* **1997**, *109*, 1513; *Angew. Chem. Int. Ed. Engl.* **1997**, *36*, 1445.

[20] a) F. Bottomley, C. P. Magill, B. Zhao, *Organometallics* **1990**, *9*, 1700; b) F. Bottomley, C. P. Magill, B. Zhao, *Organometallics* **1991**, *10*, 1946; c) F. Bottomley, P. D. Boyle, S. Karslioglu, *Organometallics* **1993**, *12*, 4090; d) C. E. Dubé, D. W. Wright, S. Pal, Bonitatebus, Jr., W. H. Armstrong, *J. Am. Chem. Soc.* **1998**, *120*, 3704.

[21] a) M. Descostes, F. Mercier, N. Thromat, C. Beaucaire, M. Gautier-Soyer, *Appl. Surf. Sci.* **2000**, *165*, 288; b) L. Legrand, A. E. Figuigui, F. Mercier, A. Chausse, *Environ. Sci. Technol.* **2004**, *38*, 4587; c) B. J. Tan, K. J. Klabunde, P. M. A. Sherwood, *Chem. Mater.* **1990**, *2*, 186.

[22] H. An, E. Wang, D. Xiao, Y. Li, Z. Su, L. Xu, *Angew. Chem.* **2006**, *118*, 918; *Angew. Chem. Int. Ed.* **2006**, *45*, 904.

[23] *Three-Dimensional Nets and Polyhedra* (Ed.: A. F. Wells), Wiley, New York, **1977**.

[24] O. V. Dolomanov, A. J. Blake, N. R. Champness, M. SchrNder, *J. Appl. Crystallogr.* **2003**, *36*, 1283.

[25] M. Du, X.-H. Bu, Y.-M. Guo, L. Zhang, D.-Z. Liao, J. Ribas, *Chem. Commun.* **2002**, 1478, and references therein.

[26] J. A. Bertrand, A. P. Ginsberg, R. I. Kaplan, K C. Eirkwood, R. L. Martin, R. C. Sherwood, *Inorg. Chem.* **1971**, *10*, 240.

[27] a) M. Mikuriya, K. Minowa, R. Nukada, *Bull. Chem. Soc. Jpn.* **2002**, *75*, 2595; b) M. P. Shores, B. M. Bartlett, D. G. Nocera, *J. Am. Chem. Soc.* **2005**, *127*, 17986; c) G. Arom, J. Ribas, P. Gamez, O. Roubeau, H. Kooijman, A. L. Spek, S. Teat, E. MacLean, H. Stoeckli-Evans, J. Reedijk, *Chem. Eur. J.* **2004**, *10*, 6476.

[28] a) L. Bi, U. Kortz, S. Nellutla, A. C. Stowe, J. van Tol, N. S. Dalal, B. Keita, L. Nadjo, *Inorg. Chem.* **2005**, *44*, 896; b) M. Murugesu, K. A. Abboud, G. Christou, *Dalton Trans.* **2003**, 4552; c) D. Foguet-Albiol, K. A. Abboud, G. Christou, *Chem. Commun.* **2005**, 4282.

[29] a) J. J. Borrás-Almenar, J. M. Clemente-Juan, E. Coronado, B. S. Tsukerblat, *Inorg. Chem.* **1999**, *38*, 6081; b) J. J. Borrás-Almenar, J. M. Clemente-Juan, E. Coronado, B. S. Tsukerblat, *J. Comput. Chem.* **2001**, *22*, 985.

[30] a) S. Konar, E. Zangrando, M. G. B. Drew, J. Ribas, N. R. Chaudhuri, *Dalton Trans.* **2004**, 260; b) T. C. Higgs, K. Spartalian, C. J. O'Connor, B. F. Matzanke, C. J. Carrano, *Inorg. Chem.* **1998**, *37*, 2263.

[31] C.-F. Wang, J.-L. Zuo, B. M. Bartlett, Y. Song, J.-R. Long, X.-Z. You, *J. Am. Chem. Soc.* **2006**, *128*, 7162.

[32] W. E. Hatfield, *Theory and Applications of Molecular Paramagnetism*, Wiley, New York, **1976**.

[33] a) C. L. Hill, C. Chrisina, M. P. McCartha, *Coord. Chem. Rev.* **1995**, *143*, 407; b) I. V. Kozhevnikov, *Chem. Rev.* **1998**, *98*, 171; c) N. Mizuno, K. Yamaguchi, K. Kamata, *Coord. Chem. Rev.* **2005**, *249*, 1944.

[34] The analogous species based on the precursors of $[\alpha\text{-}A\text{-}GeW_9O_{34}]^{10-}$, $[\gamma\text{-}SiW_{10}O_{36}]^{8-}$, $[\alpha\text{-}P_2W_{15}O_{56}]^{12-}$ and $[H_2P_2W_{12}O_{48}]^{12-}$ were also obtained under hydrothermal conditions and characterized by single-crystal X-ray diffraction in our group. Further investigation on their magnetic properties is in progress.

[35] a) G. M. Sheldrick, SHELXS97, Program for Crystal Structure Solution, University of Göttingen, Göttingen (Germany), **1997**; b) G. M. Sheldrick, SHELXL97, Program for Crystal Structure Refinement, University of Göttingen, Göttingen (Germany), **1997**.

Received: August 27, 2007
Revised: October 7, 2007
Published online: November 23, 2007

